X-linked ectodermal dysplasia and immunodeficiency caused by reversion mosaicism of NEMO reveals a critical role for NEMO in human T-cell development and/or survival

Ryuta Nishikomori, Hiroshi Akutagawa, Kyoko Maruyama, Mami Nakata-Hizume, Katsuyuki Ohmori, Kazunori Mizuno, Akihiro Yachie, Takahiro Yasumi, Takashi Kusunoki, Toshio Heike, and Tatsutoshi Nakahata

X-linked ectodermal dysplasia and immunodeficiency (XL-EDA-ID) is an X-linked recessive disease caused by a mutation in the nuclear factor–κB (NF-κB) essential modulator (NEMO). Here we report an XL-EDA-ID patient with atypical features of very few naive-phenotype T cells and defective mitogen-induced proliferation of peripheral blood mononuclear cells (PBMCs). The patient's NEMO defect was diagnosed by flow cytometric analysis of intracellular NEMO staining. Specific cell lineages (monocytes and neutrophils) expressed reduced levels of NEMO, but 2 populations of T, B, and NK cells were detected with normal and reduced expression of NEMO. Genomic analysis revealed that duplication of a 4.4-kb sequence ranging from intron 3 to exon 6 caused the reduced expression of NEMO. Polymorphism analysis showed that the patient's B- and T-cell lines with reduced and normal expression of NEMO had the same X chromosome, indicating that the somatic mosaicism was not due to feto-maternal transfusion but was most likely due to postzygotic reversion. This XL-EDA-ID case adds to our understanding of NEMO biology, indicating that NEMO is critical for T-cell development and/or survival in humans as well as in mice. (Blood. 2004;103:4565-4572)

Introduction

Ectodermal dysplasia and immunodeficiency (EDA-ID) is a disease whose clinical features include hypohidrosis, delay of eruption of teeth, coarse hair, and immunodeficiency associated with frequent bacterial infections.[1-5] Two genes responsible for EDA-ID have been identified: nuclear factor–κB (NF-κB) essential modulator (NEMO; in X-linked–EDA-ID [XL-EDA-ID])[6-8] and IκB (in autosomal-dominant EDA-ID).[9] NEMO is necessary for the function of IκB kinase, which phosphorylates and degrades IκB to activate NF-κB.[10] Thus, the defect in NEMO causes various kinds of abnormalities in signal transduction involving NF-κB, the interleukin 1 (IL-1) family protein receptors, the Toll-like receptors, vascular endothelial growth factor receptor–3 (VEGFR-3), receptor activator of nuclear factor κB (RANK), the ectodysplasin-A receptor, CD40, and the tumor necrosis factor (TNF) receptor.[11]

NEMO is also responsible for X-linked–dominant incontinentia pigmenti (IP).[12] Males with IP usually die before birth. The XL-EDA-ID cases reported so far have also been male (with one exception[13]) but have only one mutated NEMO allele. Residual NEMO activity in XL-EDA-ID and a total lack of NEMO activity in IP can explain the phenotype differences in these 2 populations of males with NEMO defects.[7,8,12] Furthermore, the majority of NEMO mutations in IP patients are large deletions due to recombination, while XL-EDA-ID patients have small mutations such as missense mutations, early stop codons, and stop codon mutations.[12,14]

The immunologic features of XL-EDA-ID reported so far consist of dysregulated immunoglobulin synthesis or hyper-immunoglobulin M (hyper-IgM) syndrome, defective antipolysaccharide antibody synthesis (antipneumococcal antibody and isohemagglutinin), reduced lipopolysaccharide (LPS) and IL-1 family protein responses, and defective natural killer (NK) cell activity.[3,4,6-8,15-19] Complete loss of NEMO function is lethal in mice due to liver failure,[20] but studies using conditional knockout mice or recombination-activating gene (RAG) chimera reconstitution have suggested that T and B cells do not develop in the complete absence of NEMO in the mouse.[21-24] Although XL-EDA-ID is phenotypically different in individuals with different NEMO mutations, there have been no XL-EDA-ID cases reported so far that show a role for NEMO in T-cell development and survival. Now we report a patient with a novel type of XL-EDA-ID whose NEMO expression varied among cell lineages due to reversion mosaicism of a 4.4-kb duplication of a portion of the NEMO gene. The patient provided us with a unique opportunity to elucidate NEMO biology in humans because in this patient we could correlate the NEMO level with cell function in various cell types. In

From the Department of Pediatrics and Laboratory Medicine, Graduate School of Medicine, Kyoto University, Kyoto, Japan; Department of Pediatrics, Hyogo Prefectural Tsukaguchi Hospital, Tsukaguchi, Japan; Department of Pediatrics, Graduate School of Medical Science, Kanazawa University, Kanazawa, Japan; and Department of Laboratory Sciences, School of Health Sciences, Faculty of Medicine, Kanazawa University, Kanazawa, Japan.

Submitted October 27, 2003; accepted January 5, 2004. Prepublished online as *Blood* First Edition Paper, January 15, 2004; DOI 10.1182/blood-2003-10-3655.

Supported by the Program for Promotion of Fundamental Studies in Health Science of the Organization for Pharmaceutical Safety and Research of Japan; a Grant-in-Aid for Creative Scientific Research (13GS0009) from the Ministry of Education, Science, Technology, Sports, and Culture of Japan; and The Shimizu Foundation Research Grant for 2003.

Reprints: Tatsutoshi Nakahata, 54 Shogoin Kawahara-cho, Sakyo, Kyoto 606-8507, Japan; e-mail: tnakaha@kuhp.kyoto-u.ac.jp.

The publication costs of this article were defrayed in part by page charge payment. Therefore, and solely to indicate this fact, this article is hereby marked "advertisement" in accordance with 18 U.S.C. section 1734.

particular, we showed that T cells with normal levels of NEMO (due to reversion) predominated over T cells with reduced levels of NEMO, indicating that NEMO is critical for human T-cell development and/or survival.

Patients, materials, and methods

Informed consent

Informed consent was obtained for the patient and his family according to the protocol of the internal review board of Kyoto University Hospital.

Proliferation assay

Peripheral blood mononuclear cells (PBMCs) were stimulated with a plate-bound antihuman CD3 monoclonal antibody (mAb; clone OKT3, 1 μg/mL; Ortho Diagnostics Systems, Raritan, NJ), a plate-bound antihuman CD3 mAb (1 μg/mL) plus a soluble antihuman CD28 mAb (clone 9.3, 2 μg/mL; kindly provided by Dr Martin Paul, Fred Hutchinson Cancer Institute, Seattle, WA), phytohemagglutinin (PHA; 1:100 dilution; Invitrogen, Carlsbad, CA), and phorbol myristate acetate (PMA; 20 ng/mL)/ionomycin (1 μM; Sigma, St Louis, MO) with or without additional IL-2 (100 IU/mL; kindly provided by Shionogi & Co, Osaka, Japan). Forty-eight hours later, ^{3}H-thymidine uptake was measured in triplicate using a 6-hour pulse of 0.5 μCi (0.0185 MBq) ^{3}H-thymidine.

Cytokine production study

PBMCs were stimulated with varying doses of IL-18 with IL-12 (20 ng/mL; R&D Systems Inc, Minneapolis, MN) or varying doses of LPS (Sigma) with interferon γ (IFN-γ; 5000 U/mL; R&D Systems Inc). Forty-eight hours later, the supernatant was harvested and the cytokines were measured using human BD OptEIA enzyme-linked immunosorbent assay (ELISA) kits (BD Biosciences Pharmingen, San Diego, CA).

Western blotting

Human T-cell lymphotropic virus I (HTLV-I)–transformed cell lines were made as previously described by Ueno et al.[25] Cell lysates (50 μg) were electrophoresed with sodium dodecyl sulfate–polyacrylamide gel electrophoresis (SDS-PAGE), and immunoblotting was performed as previously described using a mouse anti-NEMO mAb (C73-764; BD Biosciences Pharmingen) and a horseradish peroxidase (HRP)–conjugated rabbit anti-mouse IgG polyclonal antibody.[26] The same blots were reprobed with a mouse anti–β-actin mAb (AC-74; Sigma) and an HRP-conjugated goat antimouse IgG polyclonal antibody.

Flow cytometry analysis

For NEMO intracellular staining, the cells were fixed, permeabilized, washed with Permfix and Permwash (BD Biosciences Pharmingen), and stained sequentially with a mouse anti-NEMO mAb (1 μg/mL; C73-764 or clone 54; BD Biosciences Pharmingen) and a phycoerythrin (PE)–labeled goat antimouse IgG Ab (DAKO Japan Co, Kyoto, Japan). The cells were stained for the following lineage markers after staining for NEMO: CD4, CD8, CD14, CD15, CD19, CD56 (BD Biosciences Pharmingen), and IgD (DAKO Japan Co). For intracellular staining of human IFN-γ, PBMCs were stimulated with PMA/ionomycin/monensin (2 μM; Calbiochem-Novabiochem, San Diego, CA) for 6 hours, fixed, permeabilized, and stained for NEMO, human IFN-γ (BD Biosciences Pharmingen), and lineage markers, sequentially. For CD40L stimulation, PBMCs were cultured with recombinant human soluble CD40L (2.5 μg/mL; PeproTech Inc, Rocky Hill, NJ) for 48 hours; stained for CD23, CD54, CD86, CD95, and CD19 (BD Biosciences Pharmingen); fixed; permeabilized; and stained with an fluorescein isothiocyanate (FITC)–labeled rabbit anti-NEMO polyclonal antibody (Santa Cruz Biotechnology, Santa Cruz, CA). For analysis of naive T cells, PBMCs were stained with CCR7, CD45RA, and lineage makers and stained for NEMO with an FITC-labeled rabbit anti-NEMO polyclonal antibody. The stained cells were collected by FACSCalibur (BD Biosciences, San Jose, CA) and analyzed with FlowJo (Tree Star, San Carlos, CA).

Southern blotting and Northern blotting

Genomic DNA was isolated with a Puregene isolation kit according to the manufacturer's protocol (Gentra, Minneapolis, MN). DNA (5 μg) was digested with *Hin*dIII, electrophoresed, transferred to a Hybond-N nylon membrane (Amersham Biosciences, Piscataway, NJ), and cross-linked by UV irradiation. Southern hybridization was performed as previously described with a DNA probe containing exon 2 of the NEMO gene.[26] Total RNA was isolated with a Trizol RNA isolation kit according to the manufacturer's protocol (Invitrogen). Total RNA (10 μg) was electrophoresed in a formaldehyde gel, transferred to a Hybond-N nylon membrane, and cross-linked by UV irradiation. Northern hybridization was performed as previously described with a NEMO cDNA comprising NEMO exon 3.[26] The blot was stripped and reprobed with a glyceraldehyde phosphate dehydrogenase (GAPDH) cDNA as a loading control.

PCR

Genomic polymerase chain reaction (PCR) was performed using the long-range amplification system Takara LA Taq (TaKaRa Shuzo, Otsu, Shiga, Japan) with GC high buffer I according to the manufacturer's protocol. The PCR primers (Figure 3C) were as follows: NEMO1, 5′-CAATACCGAGCATCTGAGGGCAGGCACAC-3′; NEMO2, 5′-AGAGACGAAGGAGCACAAAGCTGCCTTGAG-3′; NEMO3, 5′-ACTGCAGGGACAATGGTGGGTGCATCTGTC-3′; NEMO4, 5′-TGTGGACACGCAGTGAAACGTGGTCTGGAG-3′; NEMO5, 5′-TGGCCTGCTGACACTCCTGAGAGCAACATC-3′; NEMO6, 5′-GTGGCTCAGAAGCTTACGAAAGGCCACTAC-3′; NEMO7, 5′-TGGAAGCTCAGGTGAGAGGAGAGG-3′; NEMO8, 5′-TCTTTGATACAGTCATGCCATC-TGCTCTCC-3′; and NEMO9, 5′-AGTCCCTGAGATGGAGAGAAAGGAGTATCC-3′.

The PCR cycle consisted of 94°C for 25 seconds and 68°C for 1 minute/kb with a 3-minute initial denaturation at 94°C and a 7-minute final extension at 72°C. Thirty-five cycles were used for all PCR reactions. To clone the duplicated NEMO gene, we subcloned 3 overlapping fragments using the TOPO XL PCR cloning kit (Invitrogen) and sequenced all 3 fragments with an ABI BigDye Terminator kit on an ABI3100 (Applied Biosystems, Foster City, CA). The mutation-specific PCR reaction was performed using primers NEMO8 and NEMO2 (or NEMO3), and no compatible bands were detected from any of the 20 healthy controls tested.

For the assay of the human androgen receptor trinucleotide repeat polymorphism with X inactivation, PCR was performed as previously described by Allen et al.[27] For pseudogene delta NEMO–specific PCR amplification, primer pairs NEMO9 and NEMO7 were used.

Results

Clinical and immunologic features of the patient with EDA-ID

The patient was a 2-year-old boy, born at term to healthy, nonconsanguineous parents. He had hypohidrosis, coarse hair, delayed eruption of teeth, and transient lower extremity lymphedema but did not develop the osteopetrosis or skin lesions typical of IP. At the age of 3 months, he was admitted to a local hospital because of interstitial pneumonitis. Since then he has had frequent bacterial infections and febrile episodes due to a *Staphylococcus aureus* skin abscess (7 and 9 months of age), pneumonia (13 months of age), pneumococcal sepsis (19 and 26 months of age), *Pseudomonas aeruginosa* otitis media (26 months of age), and *Pseudomonas aeruginosa* sepsis (28 months of age). In addition, he suffered from intractable diarrhea (22 months of age) that resulted

in failure to thrive. Tests for *Cryptosporidium parvum* and *Giardia lamblia* were negative in his stool. The patient received one oral live polio vaccination, which resulted in no detectable anti-polio virus titers.

The clinical symptoms described above led us to speculate that the patient had XL-EDA-ID, which is known to be caused by a mutation in NEMO. First we evaluated the patient's immunologic profile. A laboratory examination when the patient was 9 months old showed increased levels of IgG and IgA (IgG, 10.63 g/L [1063 mg/dL] [healthy controls 4.55-10.15 g/L (455-1015 mg/dL)]; IgA, 1.36 g/L [136 mg/dL] [healthy controls 0.14-0.84 g/L (14-84 mg/dL)]; IgM, 0.4 g/L [40 mg/dL] [healthy controls 0.35-1.83 g/L (35-183 mg/dL)]) but no isohemagglutinin at the age of 2.5 years and no antipneumococcal IgG2 antibody after 2 episodes of pneumococcal sepsis. C3, C4, and CH50 were within normal limits, and phagocytosis and hydrogen superoxide production by neutrophils were intact.

Notably, the patient had few $CD4^+$ cells (8%-12%), especially $CD4^+CD45RA^+$ cells (20.4% of $CD4^+$ cells), although an HIV RNA analysis was negative (Table 1). In addition, a proliferation assay showed that the patient's cells did not proliferate in response to PHA and concanavalin A (ConA; PHA, 2426 counts per minute [cpm] [healthy control 27 799-79 995 cpm]; ConA, 1230 cpm [healthy control 26 782-73 506 cpm]). These features have not previously been reported in XL-EDA-ID.

A study of the patient's cytokine response to LPS and IL-18, which activate the NF-κB signaling pathway through NEMO, showed a mixed defect (Figure 1A). LPS stimulation of the patient's PBMCs in the presence of IFN-γ caused no TNF-α secretion, while treatment with IL-18 and IL-12 induced almost as much IFN-γ as produced by healthy control cells.

Thus, the patient had both the typical immunologic features of XL-EDA-ID (recurrent streptococcal pneumoniae infections, no anti-streptococcal pneumoniae antibodies, no isohemagglutinin, and no LPS response) and atypical features (low CD4 lymphocyte concentration, differential response to LPS and IL-18, and reduced mitogen-induced proliferation).

Table 1. Surface marker analysis of the XL-EDA-ID patient's PBMCs

	%	Healthy control, %
CD3	41.2	66.1 ± 5.9
CD4	8.0	37.7 ± 9.6
CD8	31.8	23.7 ± 4.2
TCRαβ	38.0	56.5 ± 10.5
TCRγδ	3.0	9.5 ± 5.5
$CD4^+CD45RA$	1.6	32.5 ± 10.8
$CD4^+CD45RO$	7.2	10.2 ± 3.5
$CD8^+CD45RA$	32.3	20.7 ± 5.1
$CD8^+CD45RO$	9.9	7.6 ± 3.6
$CD4^+CD25^+$	2.2	5.5 ± 1.2
CD19	32.9	23.1 ± 4.1
CD20	32.6	23.3 ± 4.0
CD19/Sm-IgG	0.2	1.2 ± 1.0
CD19/Sm-IgA	0.4	0.6 ± 0.5
CD19/Sm-IgM	32.1	21.0 ± 3.8
CD19/Sm-IgD	32.1	20.8 ± 3.7
CD16	25.0	10.5 ± 5.2
CD56	24.9	9.2 ± 4.8

Surface markers of the XL-EDA-ID patient PBMCs are shown as a percentage of gated mononuclear cells. Health control values are based on 1- to 6-year-old children for whom informed consent was obtained. Health control values are shown as mean ± SD. Sm indicates surface membrane.

Reduced protein expression of NEMO in EBV-transformed but not HTLV-I–transformed cells obtained from the patient

The NEMO gene is located on the X chromosome and the patient had a 46XY karyotype as confirmed by a G-banding chromosome analysis and an XY fluorescence in situ hybridization (FISH) study of his PBMCs. We sequenced a NEMO cDNA and PCR-amplified genomic DNA from the patient's PBMCs that corresponded to the cDNA. The DNA at first seemed to be intact and did not contain the NEMO mutations in the coding region and the stop codon that have been reported previously in XL-EDA-ID.[6-8,11] In a complementary approach to define the defect, we performed Western blotting for NEMO expression (Figure 1B). We found reduced expression but not an absolute loss of NEMO in the patient's PBMCs. We then checked NEMO expression in an Epstein-Barr virus (EBV)–transformed cell line and an HTLV-I–transformed cell line derived from the patient's PBMCs. Surprisingly, the patient's HTLV-I–transformed cell lines expressed as much NEMO protein as healthy control HTLV-I–transformed cell lines, while the patient's EBV-transformed cell line expressed no or very little NEMO protein. These data suggested that the differential response to LPS and IL-18 could be derived from the differential expression of NEMO protein among these lineages.

Analysis of NEMO expression by flow cytometry

To further analyze cell lineage–specific NEMO expression, we performed intracellular staining for NEMO and flow cytometry analysis at the single-cell level. As shown in Figure 2A, flow cytometry showed a lower expression of NEMO in the patient's EBV-transformed cells than in the EBV-transformed cells of healthy controls. This is consistent with the reduced expression of NEMO seen with Western blotting. In contrast, the NEMO expression level in HTLV-I–transformed cells was similar between the patient and healthy controls.

In further studies along these lines, we measured NEMO expression in each PBMC lineage by flow cytometry. As shown in Figure 2B, healthy controls displayed a single peak of NEMO expression in all cells. In contrast, there were 2 peaks of NEMO expression in the patient's $CD4^+$, $CD8^+$, $CD19^+$, and $CD56^+$ cells and virtually no NEMO expression in the patient's $CD14^+$ and $CD15^+$ cells. Furthermore, the main population of $CD4^+$ and $CD8^+$ T cells had normal levels of NEMO ($NEMO^{normal}$), while the $CD19^+$ cells had a reduced level of NEMO ($NEMO^{low}$), and $CD56^+$ cells were almost equally divided between normal and low NEMO expression. Thus, the patient's cells had levels of NEMO expression that varied between cell lineages and even in the same cell lineages there were sometimes 2 peaks of NEMO expression.

Molecular mechanism underlying the reduced expression of NEMO

To elucidate the mechanism underlying this chimeric NEMO expression, we performed Southern blotting of the NEMO gene using exon 2 DNA as a probe. We chose exon 2 because the NEMO pseudogene, which is almost identical to the NEMO gene, does not contain exon 1 to exon 2 (Figure 3F). As shown in Figure 3A, analysis of the patient's EBV-transformed cells yielded a 15-kb band instead of the 11-kb band that was detected in healthy controls; both bands were present in his mother's cells. The patient's HTLV-I–transformed cells had the 11-kb band, which correlated with the normal protein expression of NEMO. To evaluate the NEMO mRNA level in these cells, we performed

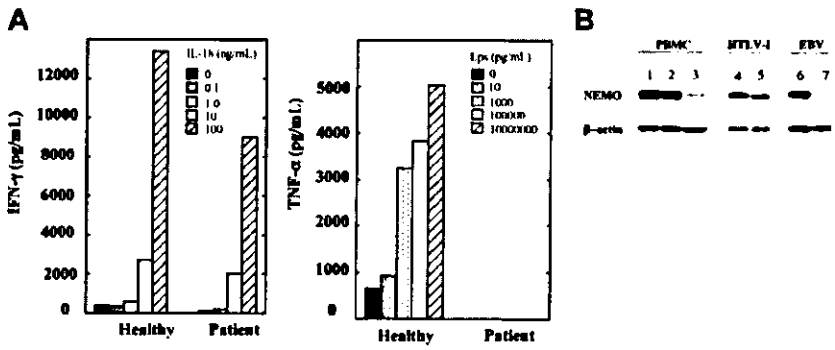

Figure 1. The differential responses of the patient's PBMCs are due to differential expression of NEMO in each lineage. (A) Defective response of the patient's PBMCs to LPS but not to IL-18. PBMCs from the patient and healthy controls were stimulated with varying doses of IL-18 plus IL-12 (20 ng/mL) or with varying doses of LPS plus IFN-γ (5000 U/mL). A representative of 2 consistent results is shown. (B) Western blotting analysis of NEMO. Fifty micrograms of PBMC cell lysates (lanes 1-3), HTLV-I–transformed cells (lanes 4-6), and EBV-transformed cells (lanes 6-7) from the patient (lanes 3, 5, and 7) and healthy controls (lanes 1, 2, 4, and 6) were used. β-actin was used as a control for equal loading (lanes 1-7).

Northern blotting on the patient's EBV-transformed cells and HTLV-I-transformed cells. As shown in Figure 3B, the patient's EBV-transformed cells expressed a much-reduced amount of NEMO mRNA, while the HTLV-I-transformed cells expressed a normal amount of NEMO mRNA. To identify the aberrant sequence, we performed genomic PCR of the patient's EBV-transformed cells using primers in intron 2 (NEMO1) and intron 8 (NEMO7), which do not amplify the NEMO pseudogene (Figure 3C,F). We obtained a 13-kb band from the EBV-transformed cells and a 9-kb band from healthy control cells and the patient's HTLV-I–transformed cells (Figure 3C). To identify the region in which the extra sequence was located, we performed PCR using the intron 2 primer and various 3′ primers (at intron 3 [NEMO2], intron 4 [NEMO3], intron 5 [NEMO4], intron 6 [NEMO5], and intron 7 [NEMO6]; Figure 3D). We obtained bands that were approximately 4-kb larger when using the 3′ primers at intron 6, intron 7, and intron 8, indicating that the extra sequence was inserted between intron 5 and intron 6. In contrast, when we performed PCR amplifying the sequence between the 3′ primers at intron 5 (NEMO8) and intron 6 (NEMO5) (Figure 3E), no size differences in the major bands were detected between EBV-transformed cells from healthy controls and the patient's cells. We also performed a restriction enzyme digestion analysis (*PstI*, *SacI*, *BglII*) to compare the 9-kb and 13-kb bands obtained from the EBV-transformed cells (Figure 3C) after isolation of both bands, which showed that the digested bands were almost identical (data not shown). These data led us to speculate that the insertion sequence could be a duplication of the 5′ adjacent sequence. To test this hypothesis, we performed PCR at the 5′ region adjacent to intron 5 using 5′ reverse (NEMO2 and NEMO3) and 3′ forward (NEMO8) primers (Figure 3E-F). As in Figure 3E, we obtained bands from the patient's EBV-transformed cells and his mother's EBV-transformed cells (data not shown) but not from healthy controls (20 healthy controls checked). We sequenced the patient-specific band and found that the third base of exon 6 (nucleotide 19 426, GenBank accession number AJ271718) was connected to intron 3 (nucleotide 14 961). We sequenced the whole 13 kb using 3 overlapping fragments, which revealed the duplication of a 4.4-kb sequence including the region from intron 3 to exon 6. Sequencing analysis demonstrated that the NEMO gene of the patient's HTLV-I–transformed cells was intact. Thus, the reduced expression of NEMO in the EBV-transformed cells was due to insertion of a duplicated sequence spanning intron 3 to exon 6 (Figure 3F).

A mutated X-chromosome allele was shared by cell lines with normal and reduced NEMO expression: reversion mosaicism

To identify the sources of the cells expressing normal and reduced amounts of NEMO, we used a genetic polymorphism on the X chromosome (Figure 4A). Analysis of the human androgen receptor trinucleotide repeat polymorphism showed that the patient carried the same allele from his mother in both HTLV-I–transformed cells with normal levels of NEMO and EBV-transformed cells with reduced levels of NEMO and did not carry the other allele from his mother nor the allele from his father. Thus,

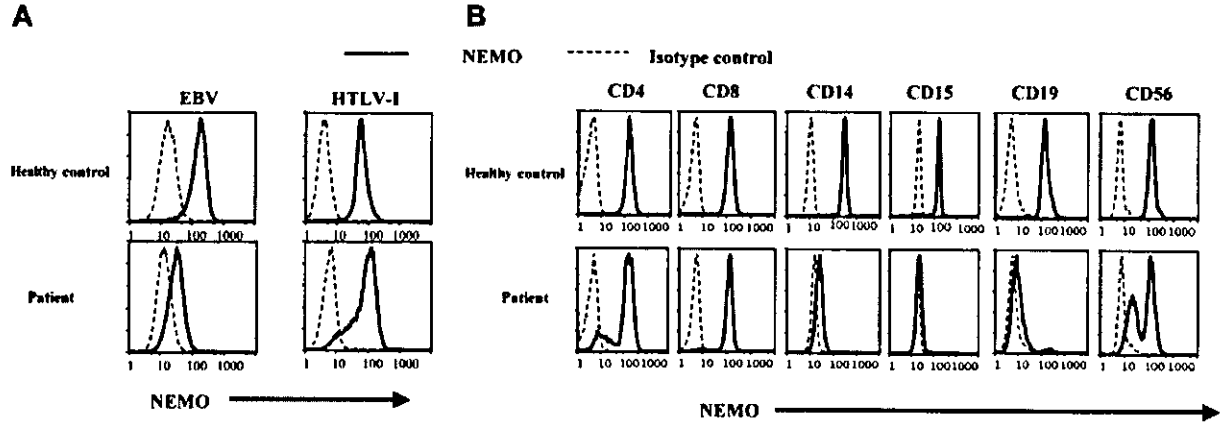

Figure 2. Analysis of NEMO protein expression using intracellular staining and flow cytometry. (A) Intracellular staining of NEMO in EBV-transformed and HTLV-I–transformed cell lines. Solid lines indicate the anti-NEMO mAb, and dotted lines indicate the isotype controls. We confirmed the NEMO specificity with 2 different anti-NEMO mAbs (C73-764, BD; or clone 54, BD) and obtained identical results. (B) Intracellular staining for NEMO in PBMCs from the patient and healthy controls. The results shown were gated on lineage markers. We performed intracellular staining on PBMCs from 10 different healthy controls, all of which showed specific staining for NEMO on every lineage tested.

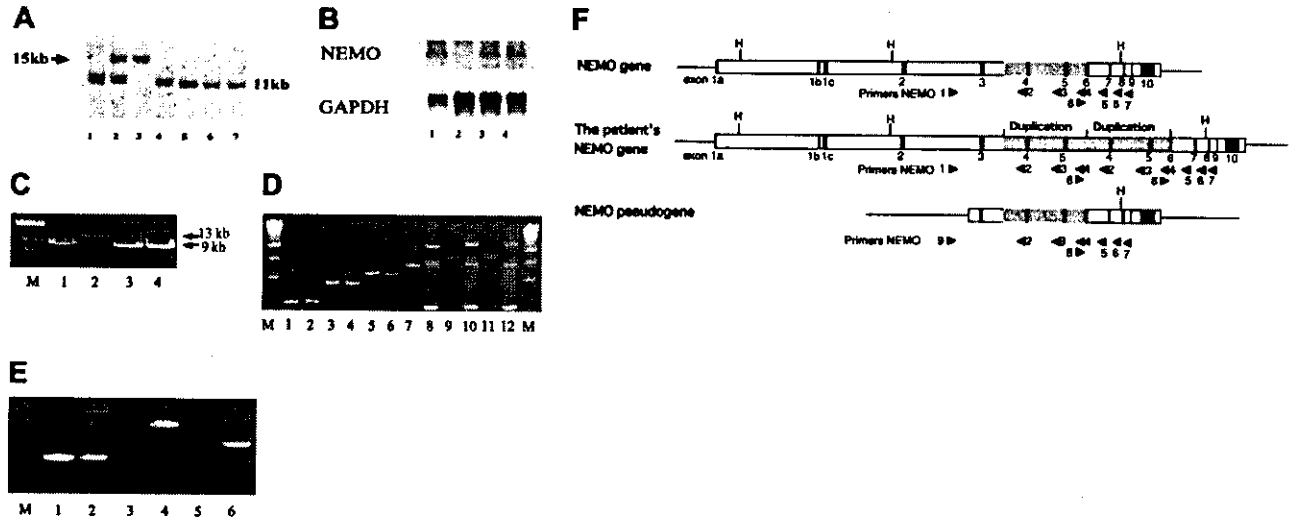

Figure 3. Reduced NEMO expression was caused by duplication of the NEMO gene. (A) Southern blotting analysis of the NEMO gene. Genomic DNA was digested with *Hin*dIII and electrophoresed, and the blot was hybridized with exon 2 DNA as a probe. DNA from the patient's EBV-transformed cells (lane 3) showed a 15-kb band, which was shared by his mother (lane 2), instead of the 11-kb bands, which were detected in the DNA from the patient's HTLV-I–transformed cells (lane 4), his father's EBV-transformed cells (lane 1), his mother's EBV-transformed cells (lane 2), and EBV-transformed cells from healthy controls (lanes 5-7). (B) Northern blotting analysis of the NEMO gene. The blot was hybridized with exon 3 DNA as a probe. RNA from the patient's EBV-transformed cells (lane 2) expressed very little NEMO mRNA compared with his HTLV-I–transformed cells (lane 1) and the EBV-transformed cells from healthy controls (lanes 3-4). (C) PCR reaction using primers 1 and 7. Only the NEMO gene was amplified. EBV-transformed cells (lane 2) had a 13-kb band instead of the 9-kb band seen in HTLV-I–transformed cells (lane 1) and healthy controls (lanes 3-4). M indicates lambda/*Hin*dIII digestion marker. (D) PCR reaction using primers 1 and 2 (lanes 1-2), primers 1 and 3 (lanes 3-4), primers 1 and 4 (lanes 5-6), primers 1 and 5 (lanes 7-8), primers 1 and 6 (lanes 9-10), and primers 1 and 7 (lanes 11-12). The patient's EBV-transformed cells (lanes 2, 4, 6, 8, 10, and 12) and those of healthy controls (lanes 1, 3, 5, 7, 9, 11) were used as templates. The larger bands detected in lanes 8, 10, and 12 indicate that the insertion is between primers 4 and 5 (between introns 5 and 6). M indicates 2.5-kb ladder. (E) PCR reaction using primers 8 and 5 (lanes 1-2), primers 8 and 3 (lanes 3-4), and primers 8 and 2 (lanes 5-6). The patient's EBV-transformed cells (lanes 2, 4, and 6) and those of healthy controls (lanes 1, 3, and 5) were used as templates. M indicates 1-kb marker. (F) Schematic representation of the normal NEMO gene, the patient's NEMO gene, and the NEMO pseudogene. Primers are shown as triangles. The duplicated region found in the patient is shaded. H indicates *Hin*dIII digestion sites.

expansion of maternal cells after fetomaternal transfusion was unlikely (also confirmed by FISH with a Y probe). An X-inactivation assay showed that the allele shared by the patient and his mother was methylated and inactivated in the mother's cells (Figure 4A). Furthermore, both the patient's EBV-transformed cells and HTLV-I–transformed cells have the same single-nucleotide polymorphism found in his mother's NEMO pseudogene, corresponding to exon 8 of the NEMO coding region (Figure 4B). Taken together, these data strongly imply that the patient's normal and duplicated NEMO genes were derived from the same X chromosome, indicating that postzygotic reversion was responsible for the somatic cell NEMO mosaicism.

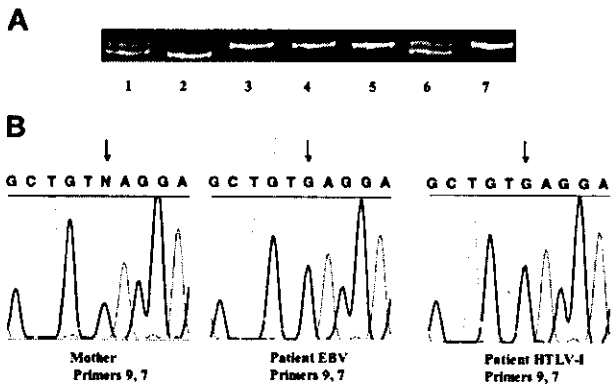

Figure 4. Reversion mosaicism of NEMO. (A) Human androgen receptor trinucleotide repeat polymorphism. Cells from the patient's mother (lanes 1, 6, and 7), the patient's father (lane 2), and the patient (PBMCs, lane 3; EBV-transformed cells, lane 4; and HTLV-I–transformed cells, lane 5) were used as templates. The patient's cells all had the same allele, which matched one of his mother's. This allele was methylated and inactivated in the mother, which was shown by an X-inactivation assay using *Hpa*II (with *Hpa*II, lane 7; without *Hpa*II, lane 6). (B) A single-nucleotide polymorphism in the pseudogene delta NEMO in the patient and his mother. The mother is heterozygous G/C, whereas both EBV- and HTLV-I–transformed cells from the patient had G. The arrows indicate the single-nucleotide polymorphism.

Immunologic re-evaluation of the XL-EDA-ID with NEMO gene duplication

Given the conclusion of postzygotic reversion, we were in a unique position to correlate NEMO expression with cellular function using $NEMO^{normal}$ and $NEMO^{low}$ cells (T, B, and NK cells) developing in the same environment. Thus, we re-evaluated the patient's immunologic phenotype, focusing on the expression level of NEMO, to explore the unique characteristics of this XL-EDA-ID patient (reduced mitogen-induced proliferation, low CD4 lymphocyte number in PBMCs, and relatively higher serum IgG concentration).

Since the CD40-CD40L system, and especially the NF-κB pathway, is important for immunoglobulin class switching,[28] XL-EDA-ID patients usually have normal-to-reduced IgG levels.[6-8,15,17] We examined the CD40 signaling pathway of the patient's B cells by stimulating the patient's PBMCs with recombinant human soluble CD40L (Figure 5A). Because the patient's B cells contained $NEMO^{low}$ and $NEMO^{normal}$ cells, we compared control $CD19^+$ cells and the patient's $NEMO^{low}$ $CD19^+$ cells. While recombinant human soluble CD40L induced less up-regulation of CD23, CD54, CD86, and CD95 in the patient's $NEMO^{low}$ $CD19^+$ cells than in control $CD19^+$ cells, CD40L signaling was conserved to some extent in the patient's $NEMO^{low}$ B cells.[7,8] Next we examined NEMO expression on $CD19^+IgD^+$ mature B cells and $CD19^+IgD^-$ class-switched B cells in the patient. As shown in Figure 5B, the majority of $CD19^+IgD^-$ cells were $NEMO^{normal}$, while $CD19^+IgD^+$ cells were $NEMO^{low}$. These data suggest that the increased level of

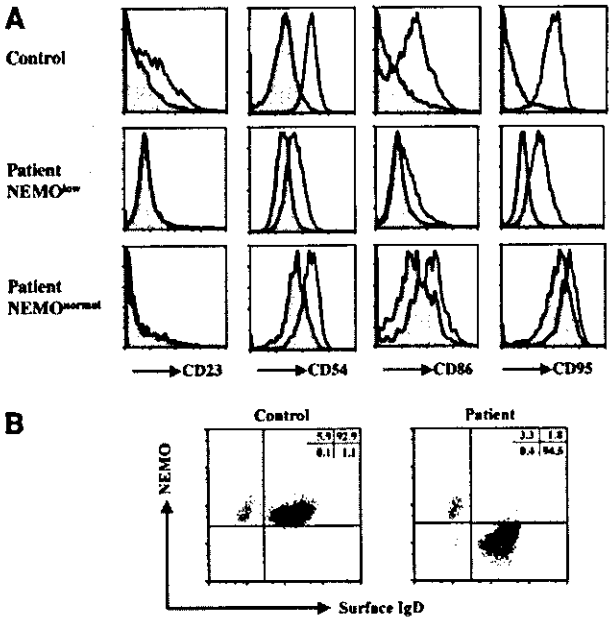

Figure 5. Analysis of the XL-EDA-ID patient's B cells. (A) Recombinant human soluble CD40L stimulation of the patient's B cells induced CD23, CD54, CD86, and CD95 up-regulation to a lesser extent. PBMCs from the patient and healthy controls were treated with (open histograms) or without (shaded histograms) recombinant human soluble CD40L (2.5 μg/mL) for 48 hours. Histograms are shown gated on $CD19^+$ cells of a control, $CD19^+NEMO^{low}$, and $CD19^+NEMO^{normal}$ cells of the patient. (B) IgD^-CD19^+ class-switched B cells were $NEMO^{normal}$. PBMCs from the patient and healthy controls were stained with CD19, NEMO, and IgD, and $CD19^+$-gated cells are shown.

IgG arises mainly from $CD19^+IgD^-NEMO^{normal}$ reverted cells, even though these cells were a minority of the B-cell population.

The patient's $CD4^+$ and $CD8^+$ T cells were composed mainly of $NEMO^{normal}$ cells, which indicated that low levels of NEMO are disadvantageous for the development and/or survival of T cells. On the other hand, even though the majority of T cells were $NEMO^{normal}$, the patient's cells displayed reduced mitogen-induced proliferation and the patient had low numbers of $CD4^+$ lymphocytes. To elucidate the mechanism underlying these findings, we performed a T-cell receptor Vβ (TCR Vβ) repertoire analysis to see whether normal T-cell development occurred after the reversion events (Figure 6A). While the $CD4^+$ T cells consisted of relatively varied types of Vβ-expressing T cells, 58% of the $CD8^+$ T cells were $V\beta16^+$, which indicated that T-cell development was impaired. The marker analysis of this repertoire showed they were $CD28^-$, $CD27^-$, $CD57^+$, $CD62L^{low}$, $CCR7^-$, $CD45RO^-$, and $CD45RA^+$, which is a $CD8^+$ memory/effector phenotype (data not shown).[30] In addition, naive-phenotype $CD4^+$ T cells ($CD45RA^+$, $CCR7^+$) and naive-phenotype $CD8^+$ T cells ($CD45RA^+$, $CCR7^+$) with either reduced or normal NEMO expression were markedly reduced in number (1.7% of $NEMO^{normal}$ $CD4^+$ cells, 3.9% of $NEMO^{low}$ $CD4^+$ cells, 0.4% of $NEMO^{normal}$ $CD8^+$ cells, and 14.3% of $NEMO^{low}$ $CD8^+$ cells; Figure 6B). To explore the functional aspects of these T cells, we performed intracellular cytokine staining for IFN-γ. As shown in Figure 6C, reverted $NEMO^{normal}$ cells (both CD4 and CD8) produced more IFN-γ than control cells, while $NEMO^{low}$ cells produced reduced amounts of IFN-γ. Thus, NEMO is critical both for the production and/or survival of T cells

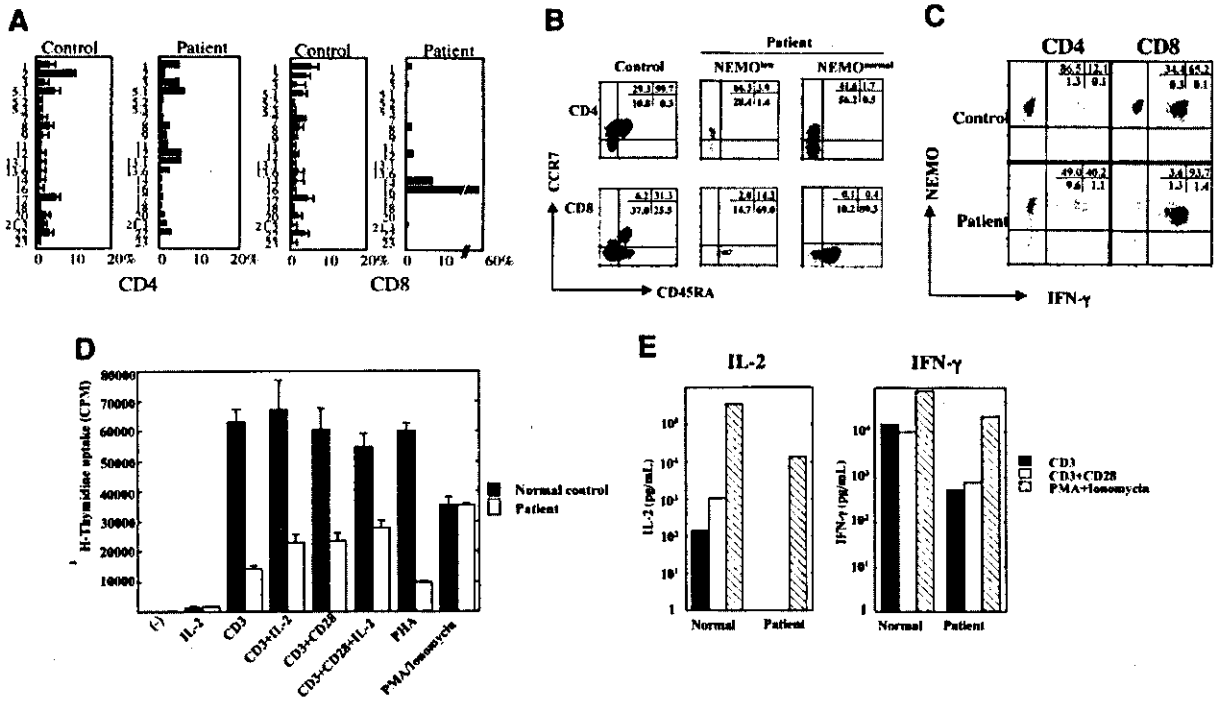

Figure 6. Analysis of the XL-EDA-ID patient's T cells. (A) TCR Vβ repertoire analysis of the patient's $CD4^+$ and $CD8^+$ cells. The patient's PBMCs were stained for the TCR Vβ panel and CD4 or CD8 as described by Kobayashi et al.[29] The healthy controls consisted of children 1 to 10 years old (n = 10). The values are shown as mean ± SD. (B) Naive and memory phenotypes of the patient's T cells. PBMCs from the patient and control were stained with NEMO, CCR7, CD45RA, and CD4 or CD8. Cells gated on $NEMO^{low}$ or $NEMO^{normal}$ of CD4 or CD8 are shown. (C) Reduced IFN-γ production of $NEMO^{low}$ T cells. The patient and control PBMCs were stimulated with PMA/ionomycin/monensin for 6 hours and stained for intracellular IFN-γ along with NEMO and CD4 or CD8. Cells gated on CD4 or CD8 are shown. (D) Proliferation assay of PBMCs stimulated by an anti-CD3 mAb plus an anti-CD28 mAb. PBMCs from the patient or healthy controls were stimulated for 48 hours with an anti-CD3 mAb, an anti-CD3 mAb plus the anti-CD28 mAb ± IL-2 (100 IU/mL), PHA, or PMA/ionomycin. Data are shown as mean ± SD. (E) Reduced production of IL-2 and IFN-γ by anti-CD3 mAb plus anti-CD28 mAb. PBMCs from the patient or healthy controls were stimulated for 48 hours by the anti-CD3 mAb, anti-CD3 mAb plus anti-CD28 mAb, or PMA/ionomycin, and the supernatants were harvested for ELISA assays.

and for the development of IFN-γ–producing T cells. In addition, the abnormal T-cell repertoire, especially of $CD8^+$ cells, and the reduced number of naive T cells showed that T-cell development was impaired, although the majority of the T cells were $NEMO^{normal}$.

Finally, we re-evaluated the proliferation potential of the T cells using an anti-CD3 mAb and an anti-CD28 mAb as stimulants, since reduced costimulatory molecule expression on B cells has been reported in XL-EDA-ID patients[7,8] and was shown in the patient under study (Figure 5B). The patient's cells did not proliferate as well as the healthy control's cells in response to the anti-CD3 mAb, while the addition of the anti-CD28 mAb or IL-2 increased the proliferation capacity (Figure 6D). It is known that memory phenotype $CD4^+$ and $CD8^+$ T cells are poor IL-2 producers.[30,31] Therefore we performed a cytokine secretion study, which showed that IL-2 production was reduced even after treatment with the anti-CD28 mAb, although the reduction in IFN-γ production was less prominent (Figure 6E). Thus, both defects in costimulation and IL-2 production contributed to the diminished mitogen-induced proliferation.

Discussion

Reversion mosaicism has been reported in primary immunodeficiency syndromes such as adenosine deaminase deficiency, X-linked recessive severe combined immunodeficiency, and Wiskott-Aldrich syndrome.[32-34] However, these mutations are small, such as missense mutations, and reversion mosaicism of a large gene duplication has not been reported in primary immunodeficiency diseases. There have been some reports that large gene duplications have been followed by reversion mosaicism in mice (pink-eyed unstable),[35,36] Drosophila (white-ivory mutation),[37] and humans (Lesch-Nyhan syndrome).[38] Characteristically, the reversion rate was very high and the duplicated gene deletions were very precise. Four possible mechanisms underlying the reversion of duplicated genes may be considered: intrachromosomal exchange, unequal sister chromatid exchange, single-strand annealing, and sister chromatid conversion.[39,40] In our case, HTLV-I–transformed cells had a normal NEMO gene as confirmed by sequence analysis, and cells with the gene reversion expressed the same amount of NEMO protein as healthy control cells (Figure 2B). These features suggest that the exact deletion of the gene duplication had also occurred in the patient.

The duplication of the NEMO gene extending from intron 3 to exon 6 greatly reduced the expression of NEMO protein. Using the gene structure prediction program GENSCAN,[41] we speculated that the duplication would insert exon 4 and exon 5 between exons 5 and 6. This would cause the NEMO protein to be truncated to 223 amino acids with the addition of 9 new amino acids as a result of a frameshift (K224fsX9, new peptide NRWLRTRPL), which is similar to the dominant-negative form of NEMO.[42] It should be pointed out that the patient's mother had completely skewed X-inactivation (also confirmed by intracellular NEMO staining, no $NEMO^{low}$ cells in the mother's PBMCs), which is not typical of XL-EDA-ID cases.[15,16] Furthermore, the appearance of transient lymphedema in the patient implied that the NEMO defect of the patient was profound.[8] Although alternative explanations exist for the reduced expression of NEMO, such as enhancer/silencer effects of the inserted sequence or changes in the stability of NEMO mRNA, we suspect that the NEMO mutation described here is the most detrimental among XL-EDA-ID cases in terms of NEMO residual activity.

It has been reported that genetically mutated mice with reduced NF-κB activity show abnormalities in T-cell development, T-cell proliferation, IL-2 production, and survival of activated T cells.[43-47] Recently, Schmidt-Supprian et al[24] reported that the number of mature T cells in T-cell–specific conditional NEMO knockout mice was markedly reduced due to apoptotic death of single-positive NEMO-deficient thymocytes. This is reminiscent of our results in that the number of mature peripheral $NEMO^{low}$ (or $NEMO^{negative}$) T cells was low and the phenotype was more severe in $CD8^+$ $NEMO^{low}$ T cells than in $CD4^+$ $NEMO^{low}$ T cells (Figure 2B). Thus, the phenotype of $NEMO^{low}$ T cells in our study, which is uncharacteristic of XL-EDA-ID, can be explained by much-reduced NEMO activity as reported in previous mouse studies.[24]

Although the majority of PBMC T cells had reverted to the normal form of NEMO, $CD4^+$ and $CD8^+$ T cells (both $NEMO^{normal}$ and $NEMO^{low}$) were mainly of the memory phenotype. In addition, the TCR repertoire was skewed, especially among $CD8^+$ T cells. The frequent infections suffered by the patient could be part of the reason for the TCR repertoire skewing and the dominance of memory T cells. However, it is doubtful that frequent infection was the only reason because the TCR repertoire abnormality (also checked by CDR3 analysis; data not shown) and the lack of naive T cells were too profound. It seems more likely that the reversion in the patient was not sufficient for complete T-cell restoration and that the few reverted $NEMO^{normal}$ T cells expanded homeostatically, resulting in T cells with memory phenotype markers.[48,49] Similar $CD4^+$ lymphocytopenia and reduced mitogen-induced proliferation with a skewed CD8 Vβ repertoire has been reported in one case of reversion mosaicism of X-linked recessive severe combined immunodeficiency with reverted T cells and nonreverted B cells, monocytes, and neutrophils.[33] The similarity would indicate a requirement for NEMO in T-cell development and/or survival as observed previously for the IL-2Rγ chain.

Acknowledgments

We are grateful to T. Yorifuji, M. Mamada, and K. Kurokawa for helpful suggestions about the genetic analysis; to M. Iseki for parasite examination/identification; and to W. Strober and A. Jain for critical reading of the manuscript.

References

1. Frix CD III, Bronson DM. Acute miliary tuberculosis in a child with anhidrotic ectodermal dysplasia. Pediatr Dermatol. 1986;3:464-467.
2. Sitton JE, Reimund EL. Extramedullary hematopoiesis of the cranial dura and anhidrotic ectodermal dysplasia. Neuropediatrics. 1992;23:108-110.
3. Abinun M, Spickett G, Appleton AL, Flood T, Cant AJ. Anhidrotic ectodermal dysplasia associated with specific antibody deficiency. Eur J Pediatr. 1996;155:146-147.
4. Schweizer P, Kalhoff H, Horneff G, Wahn V, Diekmann L. Polysaccharide specific humoral immunodeficiency in ectodermal dysplasia: case report of a boy with two affected brothers. Klin Padiatr. 1999;211:459-461.
5. Abinun M. Ectodermal dysplasia and immunodeficiency [letter]. Arch Dis Child. 1995;73:185.
6. Zonana J, Elder ME, Schneider LC, et al. A novel X-linked disorder of immune deficiency and hypohidrotic ectodermal dysplasia is allelic to incontinentia pigmenti and due to mutations in IKK-gamma (NEMO). Am J Hum Genet. 2000;67:1555-1562.
7. Jain A, Ma CA, Liu S, Brown M, Cohen J, Strober W. Specific missense mutations in NEMO result in hyper-IgM syndrome with hypohydrotic ectodermal dysplasia. Nat Immunol. 2001;2:223-228.
8. Doffinger R, Smahi A, Bessia C, et al. X-linked anhidrotic ectodermal dysplasia with immunodeficiency is caused by impaired NF-kappaB signaling. Nat Genet. 2001;27:277-285.

9. Courtois G, Smahi A, Reichenbach J, et al. A hypermorphic I{kappa}B{alpha} mutation is associated with autosomal dominant anhidrotic ectodermal dysplasia and T cell immunodeficiency. J Clin Invest. 2003;112:1108-1115.
10. Yamaoka S, Courtois G, Bessia C, et al. Complementation cloning of NEMO, a component of the IkappaB kinase complex essential for NF-kappaB activation. Cell. 1998;93:1231-1240.
11. Courtois G, Smahi A, Israel A. NEMO/IKK gamma: linking NF-kappa B to human disease. Trends Mol Med. 2001;7:427-430.
12. Smahi A, Courtois G, Vabres P, et al. Genomic rearrangement in NEMO impairs NF-kappaB activation and is a cause of incontinentia pigmenti: The International Incontinentia Pigmenti (IP) Consortium. Nature. 2000;405:466-472.
13. Kosaki K, Shimasaki N, Fukushima H, Hara M, Ogata T, Matsuo N. Female patient showing hypohidrotic ectodermal dysplasia and immunodeficiency (HED-ID). Am J Hum Genet. 2001;69:664-666.
14. Aradhya S, Woffendin H, Jakins T, et al. A recurrent deletion in the ubiquitously expressed NEMO (IKK-gamma) gene accounts for the vast majority of incontinentia pigmenti mutations. Hum Mol Genet. 2001;10:2171-2179.
15. Aradhya S, Courtois G, Rajkovic A, et al. Atypical forms of incontinentia pigmenti in male individuals result from mutations of a cytosine tract in exon 10 of NEMO (IKK-gamma). Am J Hum Genet. 2001;68:765-771.
16. Mansour S, Woffendin H, Mitton S, et al. Incontinentia pigmenti in a surviving male is accompanied by hypohidrotic ectodermal dysplasia and recurrent infection. Am J Med Genet. 2001;99:172-177.
17. Orange JS, Brodeur SR, Jain A, et al. Deficient natural killer cell cytotoxicity in patients with IKK-gamma/NEMO mutations. J Clin Invest. 2002;109:1501-1509.
18. Dupuis-Girod S, Corradini N, Hadj-Rabia S, et al. Osteopetrosis, lymphedema, anhidrotic ectodermal dysplasia, and immunodeficiency in a boy and incontinentia pigmenti in his mother. Pediatrics. 2002;109:e97.
19. Carrol ED, Gennery AR, Flood TJ, Spickett GP, Abinun M. Anhidrotic ectodermal dysplasia and immunodeficiency: the role of NEMO. Arch Dis Child. 2003;88:340-341.
20. Rudolph D, Yeh WC, Wakeham A, et al. Severe liver degeneration and lack of NF-kappaB activation in NEMO/IKKgamma-deficient mice. Genes Dev. 2000;14:854-862.
21. Schmidt-Supprian M, Bloch W, Courtois G, et al. NEMO/IKK gamma-deficient mice model incontinentia pigmenti. Mol Cell. 2000;5:981-992.
22. Pasparakis M, Schmidt-Supprian M, Rajewsky K. IkappaB kinase signaling is essential for maintenance of mature B cells. J Exp Med. 2002;196:743-752.
23. Kim S, La Motte-Mohs RN, Rudolph D, Zuniga-Pflucker JC, Mak TW. The role of nuclear factor-kappaB essential modulator (NEMO) in B cell development and survival. Proc Natl Acad Sci U S A. 2003;100:1203-1208.
24. Schmidt-Supprian M, Courtois G, Tian J, et al. Mature T cells depend on signaling through the IKK complex. Immunity. 2003;19:377-389.
25. Ueno H, Matsuda S, Katamura K, Mayumi M, Koyasu S. ZAP-70 is required for calcium mobilization but is dispensable for mitogen-activated protein kinase (MAPK) superfamily activation induced via CD2 in human T cells. Eur J Immunol. 2000;30:78-86.
26. Nishikomori R, Ehrhardt RO, Strober W. T helper type 2 cell differentiation occurs in the presence of interleukin 12 receptor beta2 chain expression and signaling. J Exp Med. 2000;191:847-858.
27. Allen RC, Zoghbi HY, Moseley AB, Rosenblatt HM, Belmont JW. Methylation of HpaII and HhaI sites near the polymorphic CAG repeat in the human androgen-receptor gene correlates with X chromosome inactivation. Am J Hum Genet. 1992;51:1229-1239.
28. Hsing Y, Bishop GA. Requirement for nuclear factor-kappaB activation by a distinct subset of CD40-mediated effector functions in B lymphocytes. J Immunol. 1999;162:2804-2811.
29. Kobayashi N, Agematsu K, Nagumo H, et al. Expansion of clonotype-restricted HLA-identical maternal CD4+ T cells in a patient with severe combined immunodeficiency and a homozygous mutation in the Artemis gene. Clin Immunol. 2003;108:159-166.
30. Hamann D, Baars PA, Rep MH, et al. Phenotypic and functional separation of memory and effector human CD8+ T cells. J Exp Med. 1997;186:1407-1418.
31. Sallusto F, Lenig D, Forster R, Lipp M, Lanzavecchia A. Two subsets of memory T lymphocytes with distinct homing potentials and effector functions. Nature. 1999;401:708-712.
32. Ariga T, Kondoh T, Yamaguchi K, et al. Spontaneous in vivo reversion of an inherited mutation in the Wiskott-Aldrich syndrome. J Immunol. 2001;166:5245-5249.
33. Stephan V, Wahn V, Le Deist F, et al. Atypical X-linked severe combined immunodeficiency due to possible spontaneous reversion of the genetic defect in T cells. N Engl J Med. 1996;335:1563-1567.
34. Hirschhorn R, Yang DR, Puck JM, Huie ML, Jiang CK, Kurlandsky LE. Spontaneous in vivo reversion to normal of an inherited mutation in a patient with adenosine deaminase deficiency. Nat Genet. 1996;13:290-295.
35. Brilliant MH, Gondo Y, Eicher EM. Direct molecular identification of the mouse pink-eyed unstable mutation by genome scanning. Science. 1991;252:566-569.
36. Gondo Y, Gardner JM, Nakatsu Y, et al. High-frequency genetic reversion mediated by a DNA duplication: the mouse pink-eyed unstable mutation. Proc Natl Acad Sci U S A. 1993;90:297-301.
37. Karess RE, Rubin GM. A small tandem duplication is responsible for the unstable white-ivory mutation in Drosophila. Cell. 1982;30:63-69.
38. Yang TP, Stout JT, Konecki DS, Patel PI, Alford RL, Caskey CT. Spontaneous reversion of novel Lesch-Nyhan mutation by HPRT gene rearrangement. Somat Cell Mol Genet. 1988;14:293-303.
39. Schiestl RH, Aubrecht J, Khogali F, Carls N. Carcinogens induce reversion of the mouse pink-eyed unstable mutation. Proc Natl Acad Sci U S A. 1997;94:4576-4581.
40. Helleday T, Arnaudeau C, Jenssen D. A partial hprt gene duplication generated by non-homologous recombination in V79 Chinese hamster cells is eliminated by homologous recombination. J Mol Biol. 1998;279:687-694.
41. Burge C, Karlin S. Prediction of complete gene structures in human genomic DNA. J Mol Biol. 1997;268:78-94.
42. Manji GA, Wang L, Geddes BJ, et al. PYPAF1, a PYRIN-containing Apaf1-like protein that assembles with ASC and regulates activation of NF-kappa B. J Biol Chem. 2002;277:11570-11575.
43. Boothby MR, Mora AL, Scherer DC, Brockman JA, Ballard DW. Perturbation of the T lymphocyte lineage in transgenic mice expressing a constitutive repressor of nuclear factor (NF)-kappaB. J Exp Med. 1997;185:1897-1907.
44. Hettmann T, DiDonato J, Karin M, Leiden JM. An essential role for nuclear factor kappaB in promoting double positive thymocyte apoptosis. J Exp Med. 1999;189:145-158.
45. Ferreira V, Sidenius N, Tarantino N, et al. In vivo inhibition of NF-kappa B in T-lineage cells leads to a dramatic decrease in cell proliferation and cytokine production and to increased cell apoptosis in response to mitogenic stimuli, but not to abnormal thymopoiesis. J Immunol. 1999;162:6442-6450.
46. Senftleben U, Li ZW, Baud V, Karin M. IKKbeta is essential for protecting T cells from TNFalpha-induced apoptosis. Immunity. 2001;14:217-230.
47. Zheng Y, Vig M, Lyons J, Van Parijs L, Beg AA. Combined deficiency of p50 and cRel in CD4+ T cells reveals an essential requirement for nuclear factor kappaB in regulating mature T cell survival and in vivo function. J Exp Med. 2003;197:861-874.
48. Murali-Krishna K, Ahmed R. Cutting edge: naive T cells masquerading as memory cells. J Immunol. 2000;165:1733-1737.
49. Tanchot C, Le Campion A, Martin B, Leaument S, Dautigny N, Lucas B. Conversion of naive T cells to a memory-like phenotype in lymphopenic hosts is not related to a homeostatic mechanism that fills the peripheral naive T cell pool. J Immunol. 2002;168:5042-5046.

Cell, Vol. 119, 1001–1012, December 29, 2004, Copyright ©2004 by Cell Press

Generation of Pluripotent Stem Cells from Neonatal Mouse Testis

Mito Kanatsu-Shinohara,[1] Kimiko Inoue,[5] Jiyoung Lee,[6] Momoko Yoshimoto,[4] Narumi Ogonuki,[5] Hiromi Miki,[5] Shiro Baba,[4] Takeo Kato,[4] Yasuhiro Kazuki,[7] Shinya Toyokuni,[2] Megumi Toyoshima,[3] Ohtsura Niwa,[3] Mitsuo Oshimura,[7] Toshio Heike,[4] Tatsutoshi Nakahata,[4] Fumitoshi Ishino,[6] Atsuo Ogura,[5] and Takashi Shinohara[1,8,*]

[1]Horizontal Medical Research Organization
[2]Department of Pathology and Biology of Diseases
Graduate School of Medicine
[3]Radiation Biology Center
Kyoto University
Kyoto 606-8501
[4]Department of Pediatrics
Graduate School of Medicine
Kyoto University
Kyoto 606-8507
[5]The Institute of Physical and Chemical Research
RIKEN
Bioresource Center
Ibaraki 305-0074
[6]Medical Research Institute
Tokyo Medical and Dental University
Tokyo 101-0062
[7]Department of Molecular and Cell Genetics
School of Life Sciences
Faculty of Medicine
Tottori University, Yonago
Tottori 683-8503
Japan

Summary

Although germline cells can form multipotential embryonic stem (ES)/embryonic germ (EG) cells, these cells can be derived only from embryonic tissues, and such multipotent cells have not been available from neonatal gonads. Here we report the successful establishment of ES-like cells from neonatal mouse testis. These ES-like cells were phenotypically similar to ES/EG cells except in their genomic imprinting pattern. They differentiated into various types of somatic cells in vitro under conditions used to induce the differentiation of ES cells and produced teratomas after inoculation into mice. Furthermore, these ES-like cells formed germline chimeras when injected into blastocysts. Thus, the capacity to form multipotent cells persists in neonatal testis. The ability to derive multipotential stem cells from the neonatal testis has important implications for germ cell biology and opens the possibility of using these cells for biotechnology and medicine.

*Correspondence: takashi@mfour.med.kyoto-u.ac.jp
[8]Present address: Department of Molecular Genetics, Graduate School of Medicine, Kyoto University, Kyoto 606-8507, Japan.

Introduction

Germ cells are unique in that they have the capacity to contribute genes to offspring. Although germ cells are highly specialized cells for the generation of gametes, several lines of evidence suggest their multipotentiality. For example, teratomas are tumors containing many kinds of cells and tissues at various stages of maturation, which occur almost exclusively in the gonads (Stevens, 1984). Furthermore, primordial germ cells (PGCs) from embryos between 8.5 and 12.5 days postcoitum (dpc) give rise to pluripotent cells when cultured under appropriate conditions (Resnick et al., 1992; Matsui et al., 1992). These EG cells have differentiation properties similar to ES cells isolated from inner cell mass (Martin, 1981; Evans and Kaufman, 1981). While these observations suggest that the germline lineage retains the ability to generate pluripotent cells, it has not been possible to establish pluripotent cells from normal neonatal gonads (Labosky et al., 1994).

We recently reported the in vitro culture of mouse spermatogonial stem cells (Kanatsu-Shinohara et al., 2003a), the only type of stem cell in the body that transmits genetic information to offspring (Meistrich and van Beek, 1993; de Rooij and Russell, 2000). When neonatal testis cells were cultured in the presence of glial cell line-derived neurotrophic factor (GDNF), leukemia inhibitory factor (LIF), epidermal growth factor (EGF), and basic fibroblast growth factor (bFGF), the germ cells developed uniquely shaped colonies, and the stem cells proliferated logarithmically over a 5 month period. Upon transplantation into the seminiferous tubules of infertile mice, the cultured cells produced normal sperm and offspring, and neither somatic differentiation nor teratoma formation was observed, indicating that the cultured cells were fully committed to the germ cell lineage (Kanatsu-Shinohara et al., 2003a). This was in contrast to ES cells, which produced teratoma after being transferred into seminiferous tubules (Brinster and Avarbock, 1994). Based on these results, we named these cells germline stem (GS) cells to distinguish them from ES or EG cells. Thus, GS cells represent a third method of expanding germline cells, but they are clearly distinct from ES/EG cells in their differentiation capacity.

In this manuscript, we describe the derivation of pluripotent stem cells from the neonatal mouse testis. Neonatal testis cells were cultured in conditions similar to those used for GS cell culture. In addition to the GS cell colonies, colonies indistinguishable from ES cell colonies appeared. This second cell type could be expanded selectively under culture conditions used for ES cells. Although they produced teratomas when transplanted subcutaneously or into the seminiferous tubules of the testis, they participated in normal embryonic development following injection into blastocysts.

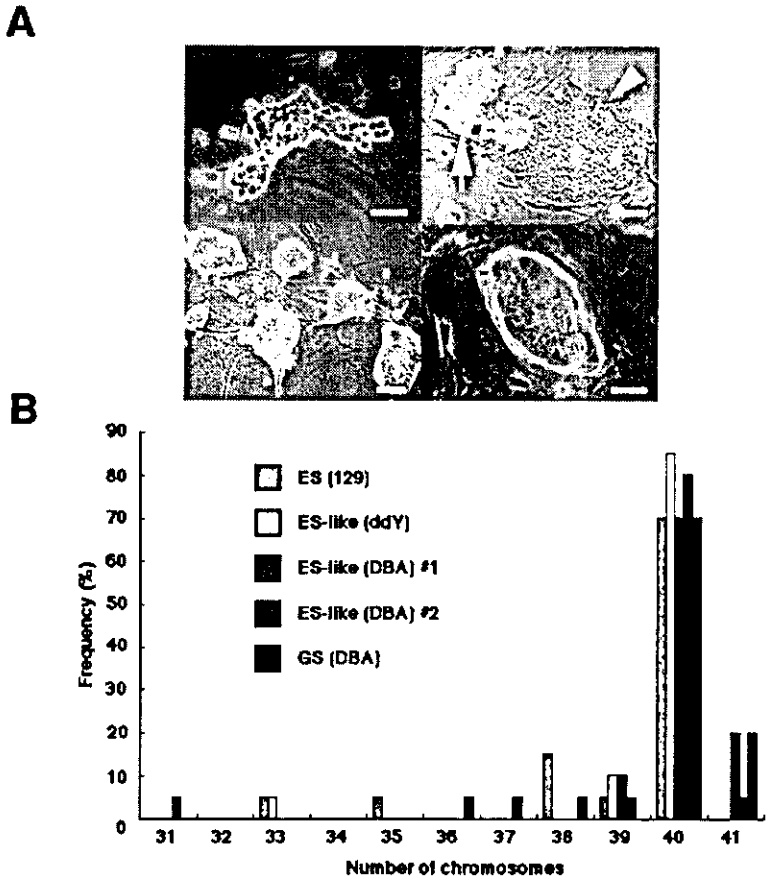

Figure 1. ES-Like Colonies from Neonatal Testis Cells

(A) Morphology of ES-like cells. (Top, left) A typical colony of GS cells. (Top, right) ES-like colony (arrow) and cultured epiblast-like colony (arrowhead), which appeared under GS cell culture conditions, at 40 days after the initiation of culture. (Bottom, left) Established culture of ES-like cells at 50 days. (Bottom, right) A typical colony of ES-like cells at 95 days.

(B) Distribution of metaphase spreads with different chromosome numbers. At least 20 cells were counted. Scale bar, 50 μm.

Results

Development of ES-Like Colonies from Neonatal Testis Cells in the Presence of Growth Factors

When neonatal ddY mouse testis cells were cultured in a primary medium containing GDNF, bFGF, EGF, and LIF, the majority of the colonies that formed had the typical appearance of GS cells, which are characterized by intercellular bridges and a morula-like structure (Figure 1A, top left) (Kanatsu-Shinohara et al., 2003a). However, we occasionally found colonies that were remarkably similar to ES cells or cultured epiblast cells (Figure 1A, top right) (Kanatsu and Nishikawa, 1996). These colonies were more tightly packed and generally appeared within 4–7 weeks after initiation of the culture (~four to seven passages). After these ES cell-like colonies appeared, they outgrew the GS cells and became the dominant population within 2–3 weeks. Although these ES-like colonies generally differentiated to lose their ES cell-like appearance after several passages under GS cell culture conditions, they retained ES-like appearance and could be selectively expanded when cultured in a secondary medium containing 15% fetal calf serum (FCS) and LIF (standard ES cell culture conditions).

After two to three passages, most colonies in the culture consisted of these ES-like colonies (Figure 1A, bottom left), which could be maintained with standard ES cell culture conditions. In contrast, GS cells could not be propagated under these conditions due to the absence of GDNF, an essential growth factor for the self-renewing division of spermatogonial stem cells (Meng et al., 2000). Cytogenetic analysis by quinacrine plus Hoechst 33258 staining showed that the ES-like cells had a normal karyotype (40, XY) in 70%–85% of metaphase spreads (Figure 1B). The morphology of the ES-like cells did not change as long as the cells were maintained in ES cell culture conditions, and they could be propagated in vitro for more than 5 months with 48 passages while maintaining an undifferentiated state (Figure 1A, bottom right). Established cultures were passed at a dilution of 1:3 to 1:6 every 3 days.

These results were reproducible; similar cells were obtained from mice with a different genotype (DBA/2), and ES-like cells were successfully established in four of 21 experiments (19%). The overall frequency of forming ES-like cells was 1 in 1.5×10^7 cells (equivalent to ~35 newborn testes). Significantly, neither GS nor ES-like cells appeared when newborn testis cells were cultured directly in ES culture conditions in at least 20 experiments. Likewise, neither GS nor ES-like cells appeared when neonatal testis cells were cultured in the presence of membrane bound Steel factor (mSCF), LIF, and bFGF (EG cell culture condition) in at least 15 experiments; the addition of GDNF was a prerequisite for the development of both GS and ES-like colonies. In addition, when CD9-selected adult spermatogonial stem cells from 3- to 8-week-old mice were cultured (Kanatsu-Shinohara et al., 2004), GS cells appeared in three of 15

experiments, but no ES-like cells appeared. We also did not observe GS or ES-like cell colonies when male genital ridges from 12.5 dpc embryos were cultured in GS cell medium in 12 experiments.

Development of ES-Like Colonies from GS Cells Derived from p53 Knockout Mice

To determine whether GS cells can convert to ES-like cells, we picked a total of 266 GS cell colonies by micromanipulation at 2 months after culture initiation. These GS cells were transferred to a 96-well plate and expanded for an additional 3 months, but none of them became ES-like cells. Although the result strongly suggested the distinct origin of ES-like cells, it was still possible that the conversion occured at lower frequency. To address this possibility, we used p53 knockout mice (Tsukada et al., 1993), which have a high frequency of testicular teratoma (Lam and Nadeau, 2003). We hypothesized that ES-like cells have a close relationship with teratoma-forming cells and asked whether established GS cells from this strain convert more easily to ES-like cells. GS cells were established from a newborn p53 knockout mouse in an ICR background. The growth speed and morphology of GS cells were indistinguishable from those of wild-type cells, and GDNF was similarly required to obtain GS cells.

Two months after culture, 30–40 GS cell colonies of undifferentiated morphology were picked by micromanipulation, transferred to a 96-well plate, and cultured in GS cell culture medium. Significantly, ES-like cells appeared in these GS cell-derived cultures in two separate experiments within 2 months, and the colonies were morphologically indistinguishable from ES-like colonies from wild-type cells. Interestingly, although ES-like cells never appeared from fully established wild-type GS cells after long-term culture, p53 knockout GS cells produced ES-like cells as long as 6 months after the initiation of culture.

Using p53 knockout mice, we also examined whether GS cells from mature testis can produce ES-like cells. Spermatogonial stem cells were collected from 3- to 8-week-old mice using anti-CD9 antibody and cultured in GS cell medium. GS cells developed in two of three experiments. GS cells of undifferentiated morphology were picked 4–7 days after culture initiation, and the colonies were expanded in vitro on mitomycin C-inactivated mouse embryonic fibroblast (MEF). In total, ES-like cells appeared in two of eight experiments within 4 weeks of culture.

Phenotypic Analysis of ES-Like Cells

To examine the phenotype of the ES-like cells, we established a population from a newborn transgenic mouse line C57BL6/Tg14(act-EGFP-OsbY01) that was bred into the DBA/2 background (designated Green). Since these Green mice express the enhanced green fluorescence protein (EGFP) gene ubiquitously, including in spermatogenic cells (Kanatsu-Shinohara et al., 2003a), cultured cells can be distinguished from feeder cells under excitation with UV light. The ES-like cells comprised a single phenotypic population by flow cytometric analysis of surface antigens (Figure 2A). They were strongly positive for SSEA-1 (ES cell marker) (Solter and Knowles, 1978), EE2 (spermatogonia marker) (Koshimizu et al., 1995), β1- and α6-integrin (GS cell marker) (Kanatsu-Shinohara et al., 2003a), CD9 (ES and GS cell marker) (Kanatsu-Shinohara et al., 2004), and EpCAM (ES and spermatogonia cell marker) (Anderson et al., 1999). The ES-like cells were weakly positive for Forssman antigen (ES cell marker) (Evans and Kaufman, 1981) and c-kit (differentiated spermatogonia marker) (Schrans-Stassen et al., 1999). In contrast, GS cells were completely negative for SSEA-1 and Forssman antigen, confirming that ES-like cells are phenotypically distinct from GS cells. GS cells from p53 knockout mice showed similar expression profile (data not shown). Although we found some expression of Forssman antigen in the neonatal testis cell population before culture, it was expressed by a non-germ cell population, and no SSEA-1-positive cells were found (Figures 2A and 2B). The ES-like cells were also strongly positive for alkaline phosphatase (ALP), which is characteristic of ES and EG cells (Resnick et al., 1992; Matsui et al., 1992) (Figure 2C).

Next, we used the reverse transcriptase-polymerase chain reaction (RT-PCR) to examine several molecules that are specifically expressed in embryonal carcinoma (EC) or ES cells. In addition to Oct-4, Rex-1, and Nanog, which are essential for maintaining undifferentiated ES cells (Pesce and Schöler, 2001; Goolsby et al., 2003; Mitsui et al., 2003; Chambers et al., 2003), the ES-like cells expressed Cripto, ERas, UTF1, Esg-1, and ZFP57 at similar levels to ES cells (Kimura et al., 2001; Takahashi et al., 2003; Okuda et al., 1998; Tanaka et al., 2002; Ahn et al., 2004). GS cells also expressed some of these molecules, but the expression was generally weaker. Significantly, we could not detect expression of Nanog in GS cells, suggesting that they have a different mechanism for self-renewal from that of ES cells (Figure 2D).

Analysis of Genomic Imprinting in ES-Like Cells

To analyze the imprinting pattern of ES-like cells, differentially methylated regions (DMRs) of three paternally imprinted regions (*H19*, *Meg3 IG*, and *Rasgrf1* regions) and two maternally imprinted regions (*Igf2r* and *Peg10* regions) were examined by bisulfite sequencing with two independent cells (Figure 3A). While the paternally imprinted regions were methylated to different degrees, the maternally imprinted regions were rarely methylated in ES-like cells. DMRs in ES cells were generally more methylated than those in ES-like cells, including maternally imprinted regions, and the DMRs of the *H19* region were methylated more extensively than the DMRs of other regions. In contrast, GS cells showed a complete androgenetic imprinting pattern: the complete methylation of both the *H19* and *Meg3 IG* DMRs and demethylation of the *Igf2r* DMR.

Next, we examined the imprint status of GS or ES-like cells from p53 knockout mice. Genomic DNA was isolated from the same cell population at four different time points during the conversion of GS cells into ES-like cells. In these experiments, the imprint status in the DMRs was determined by combined bisulfite restriction analysis (COBRA) (Xiong and Laird, 1997) (Figure 3B). As expected from the analysis of wild-type GS cells, GS

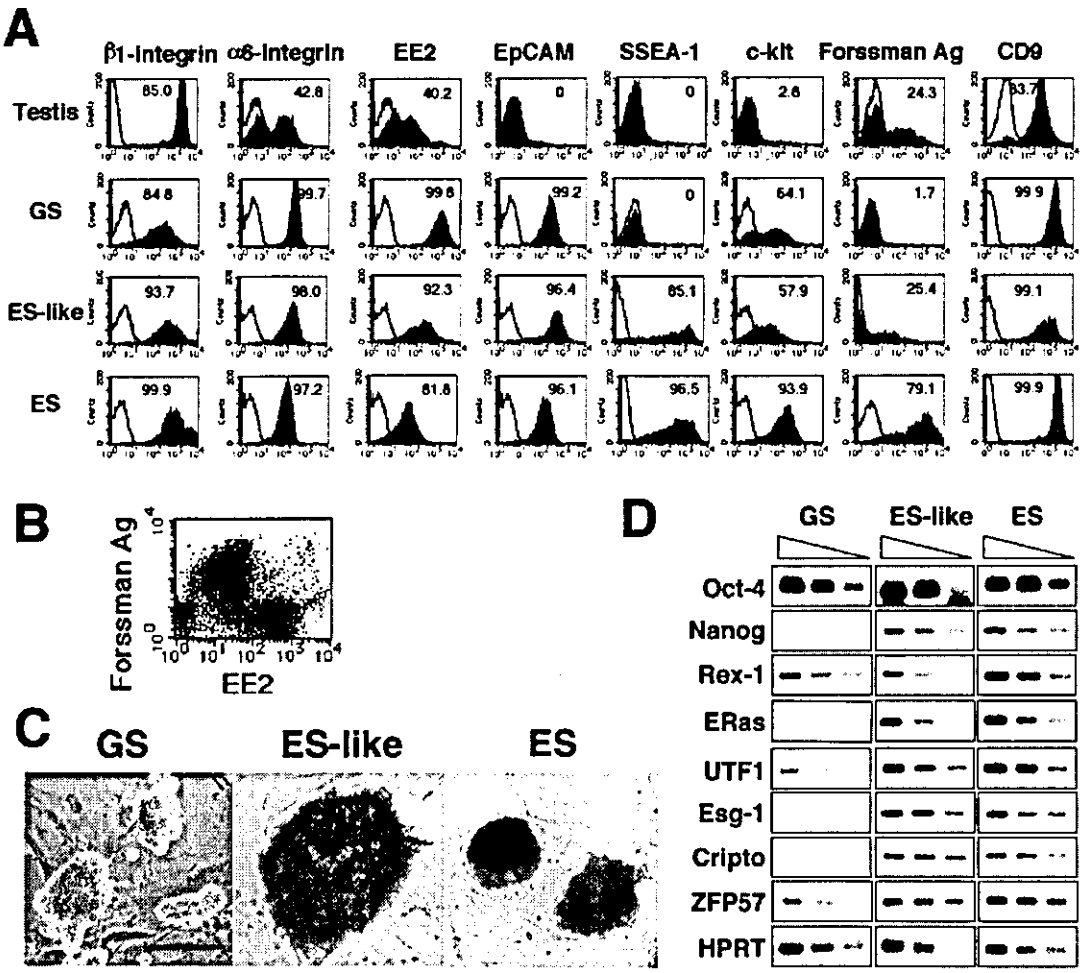

Figure 2. Phenotypic Characterization of ES-Like Cells

(A) Flow cytometric characterization of ES-like cells. Black line, control immunoglobulin; red line, specific antibody.

(B) Double immunostaining of neonatal testis cells by anti-EE2 and anti-Forssman antigen antibodies.

(C) ALP staining. GS cells (left) are weakly positive, whereas ES-like (middle) and ES cells (right) are strongly positive.

(D) RT-PCR analysis. Three-fold serial dilutions of cDNA from GS, ES-like, and ES cells were amplified with specific primers. Scale bar, 200 μm.

cells from p53 KO mice had an androgenetic imprint pattern. However, a loss of methylation in the DMRs of *H19*, *Meg 3/G*, and *Rasgrf1* regions and methylation of the DMRs in the *Igf2r* region were observed immediately after the appearance of ES-like cells. The perturbation of imprint patterns continued even when GS cells disappeared, and only the DMR of the *Peg10* region was intact, 18 days after the appearance of ES-like cells. DMR of *Oct-4* region in ES and ES-like cells were all hypomethylated, which confirms their undifferentiated state (Hattori et al., 2004) (Figure 3C).

Differentiation Potential of ES-Like Cells In Vitro and In Vivo

To determine whether ES-like cells can differentiate into somatic cell lineages, we used methods designed to induce differentiation of ES cells in vitro. ES-like cells were first transferred to an OP9 stromal feeder layer, which can support differentiation of mesodermal cells such as hematopoietic or muscle cells (Nakano et al., 1994; Schroeder et al., 2003). Within 10 days, a variety of cell types were identified including hematopoietic cells, vascular cells, and spontaneously beating myocytes (Figures 4A–4H). Hematopoiesis could also be induced when ES-like cells were cultured in methylcellulose to form embryoid bodies (Figure 4I). When we transferred ES-like cells onto gelatin-coated dishes for the differentiation of neural-lineage cells (Ying et al., 2003), they formed neurons or glial cells (Figures 4J–4L). Dopaminergic neurons were also found, albeit at low frequency (Figure 4M). When we compared the differentiation efficiency using ES cells, ES-like cells produced more glial cells than did ES cells, and there were significantly more vessel or heart muscle cell colonies from ES-like cells. However, ES-like cells could produce all of the expected lineages using protocols for ES cell differentiation (Table 1).

ES-like cells were further examined for their ability to form teratomas in vivo by subcutaneous injection into nude mice. Transplanted cells gave rise to typical teratomas in all recipients (eight of eight) by 4 weeks after transplantation (Figure 4N). The tumors contained deriv-

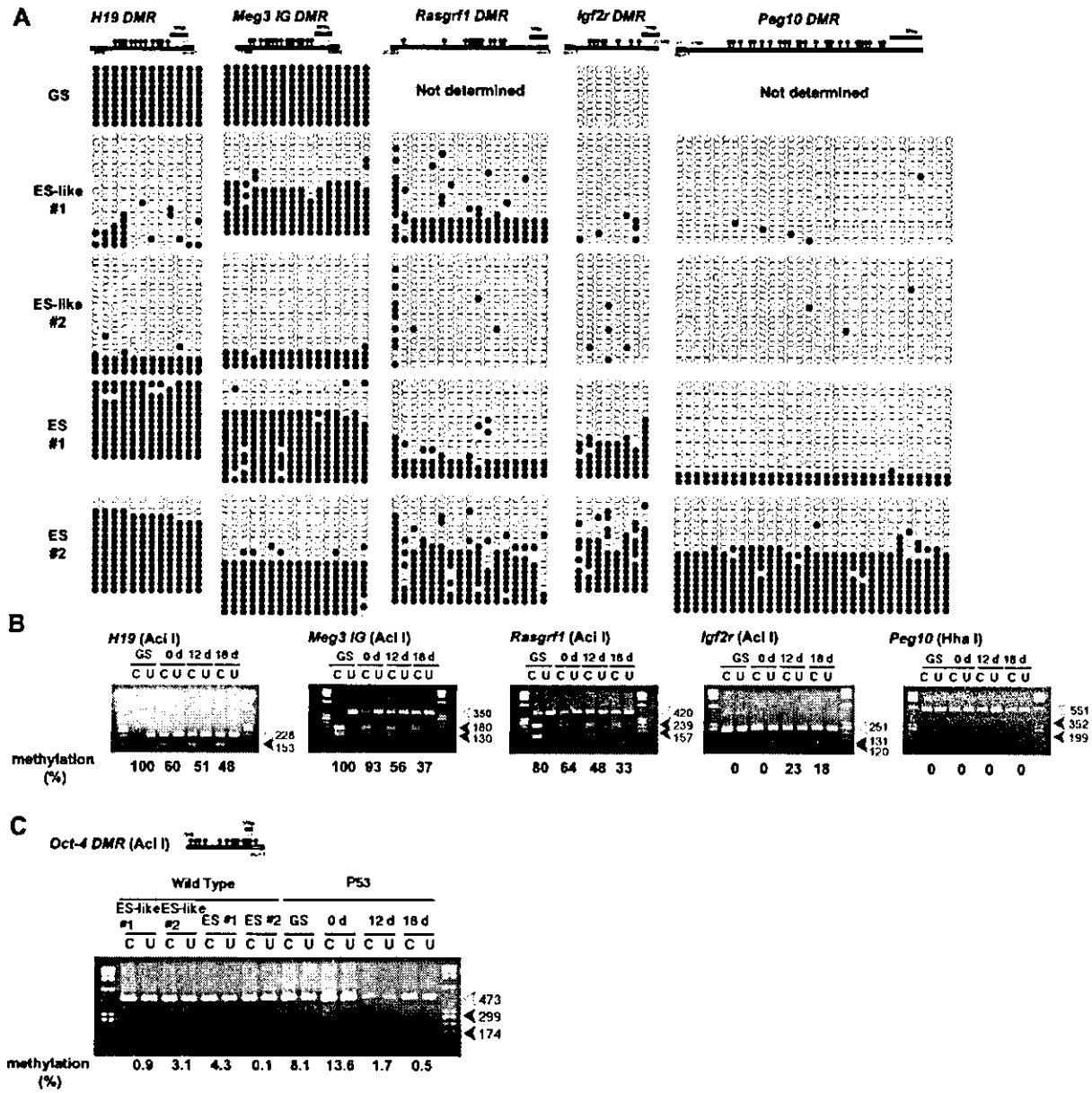

Figure 3. Analysis of Imprinting in ES-Like Cells

(A) DMR methylation of *H19, Meg3 IG, Rasgrf1, Igf2r,* and *Peg10* regions. DNA methylation was analyzed by bisulfite genomic sequencing. Black ovals indicate methylated cytosine-guanine sites (CpGs), and white ovals indicate unmethylated CpGs.

(B) COBRA of GS and ES-like cells from p53 knockout mice. The day when ES-like colonies were found was designated day 0, and cells were collected at the indicated time. In this culture, only ES-like cells were found by day 12.

(C) COBRA of *Oct-4* gene upstream region. Open arrowheads indicate the size of unmethylated DNA. Closed arrowheads indicate the size of methylated DNA. Enzymes used to cleave each locus are indicated in parentheses. U, uncleaved; C, cleaved.

atives of the three embryonic germ layers: squamous cell epithelium, neuroepithelium, and muscle. Similar results were obtained with three different clones or with ES-like cells from p53 knockout mice (eight of eight), and we did not observe a significant histological difference from teratomas derived from ES cells. In contrast, no tumors developed after transplantation of GS cells or fresh testis cells (data not shown).

Since the ES-like cells originated from testis, their ability to differentiate into germline cells was examined using the spermatogonial transplantation technique (Brinster and Zimmermann, 1994). This method allows spermatogonial stem cells to recolonize the empty seminiferous tubules of infertile animals and differentiate into mature sperm. We transplanted the cultured cells into immune-suppressed immature W mice (Kanatsu-Shinohara et al., 2003b). These mice are congenitally infertile and have no differentiating germ cells (Brinster and Zimmermann, 1994). One month after transplantation, all recipient animals (ten of ten) developed teratomas in

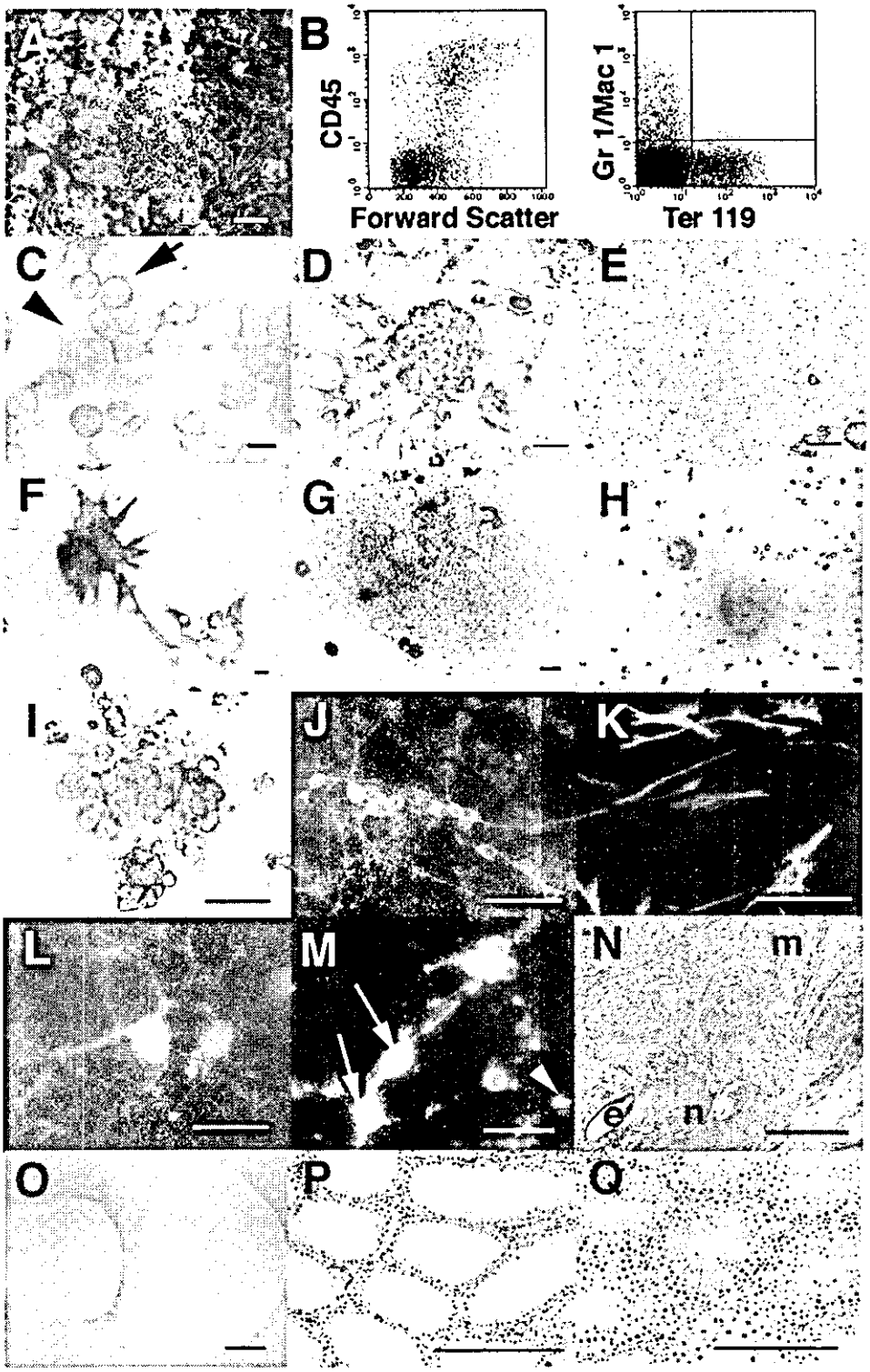

Figure 4. In Vitro and In Vivo Differentiation of ES-Like Cells

(A–H) Differentiation on OP9 cells. (A) Cobblestone formation on day 8. (B) CD45-positive hematopoietic cell development on day 7 after coculture (left). In this cell population, Gr1-positive granulocytes, Mac1-positive macrophages, or Ter119-positive erythrocytes were found (right). (C) May-Giemsa staining of harvested cells. Myeloid progenitor (arrowhead) and erythroblast (arrow) were observed. (D and E) Vascular cell differentiation. Flk-1-positive cells were sorted on day 4 after coculture, and CD31-positive (D) or VE-cadherin-positive (E) vascular cells appeared at 6 days after cell sorting. (F–H) Heart muscle differentiation. The Flk-1-positive cells were differentiated into MF20-positive (F) or cTn-I-positive (G) heart muscle at 6 days after sorting. (H) ANP-positive (blue) atrial muscle and MLC2v-positive (brown) ventricular muscle. (I) Erythroid cells that developed from embryoid body in methylcellulose at 8 days after culture. Note the red color of the cells.

(J–M) Neuronal cell differentiation on gelatin-coated plates. Tuj-positive neurons (J) on day 5, GFAP-positive astrocytes (K) and MBP-positive

Table 1. In Vitro Differentiation of ES-Like Cells from Testis

	Hematopoiesis[a,b]			Vasculogenesis[a,c]		Neurogenesis[d]		
Cell type	Increase in cell number (fold)	Granulocyte/ Macrophage (%)	Erythrocyte* (%)	Vessel*	Heart*	Neuron*	Astrocyte*	Oligodendrocyte*
ES-like	116.7 ± 15.4	7.6 ± 0.2	19.9 ± 0.7	111.5 ± 12.0	8.0 ± 4.5	126.7 ± 14.4	34.6 ± 4.4	4.6 ± 2.5
ES cell	102.3 ± 11.6	7.6 ± 0.4	24.7 ± 0.9	49.0 ± 9.2	3.8 ± 2.0	162.2 ± 14.5	10.5 ± 3.3	0.2 ± 0.1

Values are mean ± SEM. Results from at least three experiments. ES cells were derived from 129 mice, whereas ES-like cells were derived from DBA/2 mice.

[a] Flk-1-positive cells (5×10^3) were sorted 4 days after coculture and replated on OP9 feeder in a 24-well plate.

[b] Cells were recovered 7 days after sorting and analyzed by flow cytometry. Erythrocytes, macrophages, and granulocytes were identified by anti-Ter119, anti-Mac1, and anti-Gr1 antibodies, respectively.

[c] Numbers of positive cells in each well, 8 days after sorting. Vascular cells were determined by the uptake of DiI-acetylated low-density lipoprotein. Heart muscle colonies were identified by counting beating colonies.

[d] Cells (2.5×10^4) were plated on gelatin in a 48-well plate, and numbers of positive cells per cm^2 were determined by immunocytochemistry 5 (neuron) or 7 (astrocytes or oligodendrocytes) days after plating. Neurons were identified by anti-Tuj antibody, whereas astrocytes and oligodendrocytes were identified by anti-GFAP or anti-MBP antibodies, respectively. Dopaminergic neurons were produced ~10 cells per well.

* Statistically significant by Student's t test ($p < 0.05$).

the testis. The seminiferous tubules were disorganized, and no sign of spermatogenesis was found in histological sections. The cell composition found in the teratomas was similar to that of tumors that developed after subcutaneous injection (data not shown). In contrast, both wild-type and p53 KO GS cells produced normal spermatogenesis when transplanted into the seminiferous tubules (Figures 4O–4Q).

Contribution of ES-Like Cells to Normal Embryonic Development after Blastocyst Injection

Finally, we microinjected ES-like cells into blastocysts to examine whether they can contribute to chimeras in vivo. Five to fifteen cells were injected into C57BL/6 blastocysts. The ratio of euploid cells, which significantly influences the rate of chimerism or germline transmission (Longo et al., 1997; Liu et al., 1997), was 70% at the time of injection.

Some of the recipient animals were analyzed at 12.5 dpc to look for chimerism, and others were allowed to develop to term. Chimerism was observed in 25% (three of 12) of the 12.5 dpc embryos (Figure 5A) and in 36% (13 of 36) of the newborn animals (Figure 5B), as judged by the expression of EGFP observable under UV illumination. Chimerism was also confirmed by the coat color at mature stage (Figure 5C). We found six dead fetuses that showed EGFP expression, and some embryos were partially or completely absorbed. The pattern of contribution was similar at both stages analyzed; EGFP-positive donor cells were found in the central nervous system, liver, heart, lung, somites, intestine, and other tissues, including the yolk sac and chorionic membrane of the placenta (Figures 5D–5I).

Since donor cells were also found in the testis of a chimeric animal at 6 weeks of age (Figure 5J), we performed microinsemination to obtain offspring. Round spermatids were collected and microinjected into C57BL/6 × DBA/2 (BDF1) oocytes. Of 81 cultured embryos, 64 (79%) developed into 2-cells and were transferred into five psudopregnant females. Eighteen (22%) embryos were implanted, and one of the two offspring from a recipient mouse showed EGFP fluorescence, indicating the donor origin (Figure 5K). Interestingly, while control ES cells showed wide contribution to embryos, no donor cell contribution was observed in experiments using GS cells (Table 2).

To determine the full developmental potential of ES-like cells, we used tetraploid complementation technique (Nagy et al., 1993). This technique allows the production of live animals that consist entirely of donor ES cells. A total of 92 tetraploid embryos were created by electrofusion, aggregated with ES-like cells, and transferred to pseudopregnant ICR females. When some of the recipient animals were sacrificed at 10.5 dpc, we found one normal-looking fetus and several resorptions with normal placentas. The fetus showed some growth retardation but clearly expressed the EGFP gene throughout its body, including the yolk sac (Figure 5L), indicating that it was derived from donor ES-like cells. However, none of the pseudopregnant mothers sired live offspring from both ES-like and ES cells.

Discussion

The results of our experiments revealed the presence of multipotential stem cells in the neonatal testis. Although some cases of the "stem cell plasticity" phenomenon

oligodendrocytes (L) on day 7 after induction. TH and Tuj-double positive dopaminergic neurons (arrow) appeared among Tuj-positive neurons (arrowhead) (M).

(N) Section of a teratoma under the skin. The tumors contained a variety of differentiated cell types, including muscle (m), neural (n), and epithelial (e) tissues.

(O–Q) Spermatogenesis from p53 knockout GS cells. (O) A macroscopic comparison of untransplanted (left) and transplanted (right) recipient testes. Note the increased size of the transplanted testis. (P and Q) Histological appearance of the untransplanted (P) and transplanted (Q) W testes. Note the normal appearance of spermatogenesis (Q). Color staining: Cy3, red (J–M); Alexa Fluor 488, green (M). Scale bar, 50 μm (A, D–I, J, K, and M), 20 μm (C and L), 200 μm (N, P, and Q), 1 mm (O).

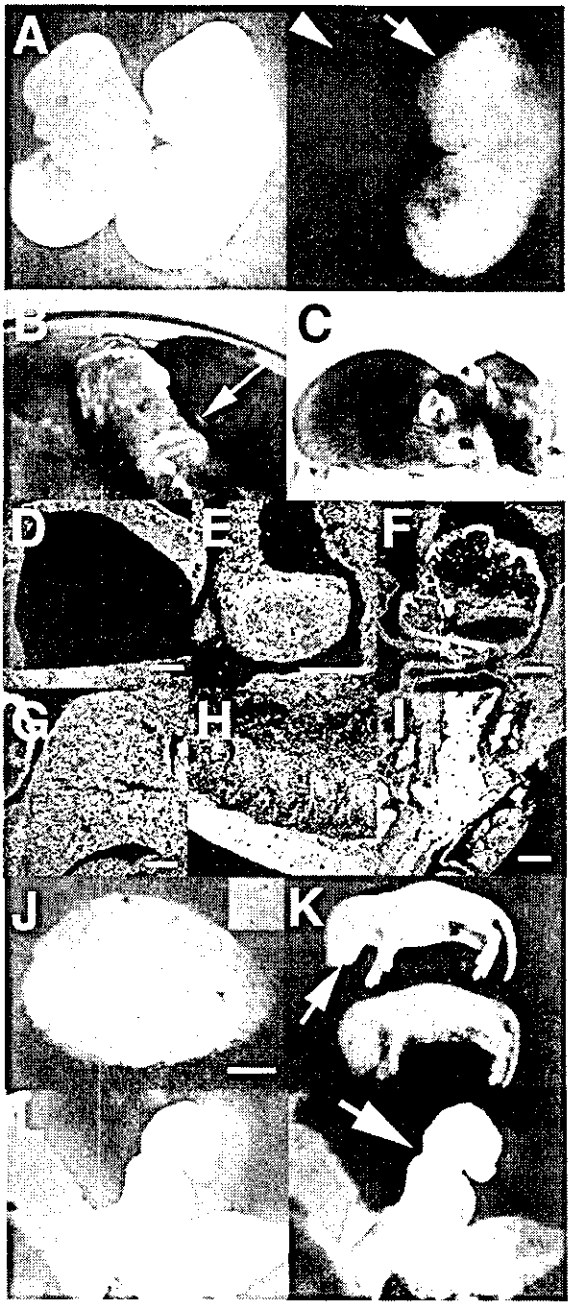

Figure 5. Production of Chimeric Animals

(A) A 12.5 dpc chimeric embryo (arrow) showing fluorescence under UV light. No fluorescence was observed in a control embryo (arrowhead).

(B) A newborn chimeric animal (arrow) showing fluorescence.

(C) Mature chimeric animals. Note the donor cell-derived coat color (cinnamon).

(D–I) Parasagittal section of a 12.5 dpc chimeric embryo. Fluorescence was observed in the brain (D), intestine (E), heart (F), liver (G), lower spinal cord (H), and placenta (I).

(J) A testis from a chimeric mouse showing fluorescence. EGFP expression was observed in some germ cells in the testis cell suspension (inset).

(K) Offspring derived from a chimera. One of the offspring showed fluorescence, confirming the donor origin (arrow).

(L) A 10.5 dpc embryo (arrow) and yolk sac produced from an aggregation of ES-like cells with tetraploid embryo showing fluorescence. No fluorescence was observed in the placenta (arrowhead). Counterstained with propidium iodide (PI) (D–I). Color staining: EGFP, green (A, B, and D–L); PI, red (D–I). Scale bar, 100 μm (D–I), 1 mm (J).

have been attributed to cell fusion (Wagers and Weissman, 2004), our case cannot be explained by the same mechanism because the ES-like cells formed teratomas after subcutaneous transplantation. These ES-like cells from the testis can be considered the neonatal counterparts of ES/EG cells. The result was unexpected, since PGCs become resistant to experimental teratocarcinogenesis or EG cell formation after 13.5 dpc (Stevens, 1984; Labosky et al., 1994). To our knowledge, EG cells are the only example of the isolation of multipotent stem cells from primary germ cells (Resnick et al., 1992; Matsui et al., 1992). EG cells were derived from primary germ cells harvested from 8.5 to 12.5 dpc fetuses and cultured in vitro with a mixture of mSCF, LIF, and bFGF. However, pluripotent cells could not be isolated from neonatal germ cells using the same culture conditions (Labosky et al., 1994), except when cells from teratomas were used (Robertson and Bradley, 1986). ES-like cells are unlikely to be derived from teratoma cells for two reasons. First, the frequency of derivation of ES-like cells in our study was significantly higher than the negligible rate of spontaneous teratoma formation in strains other than 129 and A/He mice (one teratoma out of 11,292 males in 129 hybrid backgrounds) (Stevens and Mackensen, 1961). Second, growth factor supplementation was essential for the establishment of ES-like cells. In fact, few EC cell lines have been obtained from spontaneously occurring teratocarcinomas (Robertson and Bradley, 1986). These findings strongly suggest that the ability to become multipotent stem cells persists in neonatal testis. Based on the results reported here, we propose to name these ES-like cells multipotent germline stem cells, or mGS cells, to distinguish them from GS cells, which can differentiate only into germline cells (Kanatsu-Shinohara et al., 2003a).

An important question that arises from this study is the origin of mGS cells. One possibility is that they appear independently from GS cells and originate from a population of undifferentiated pluripotent cells that persist in the testis from the fetal stage. Although EG cells have been established from ~12.5 dpc PGCs (Matsui et al., 1992; Labosky et al., 1994), cells with similar characteristics might remain in neonatal testis and produce ES-like cells. Indeed, the results of the imprinting analysis of wild-type mGS cells suggest a distinct origin for mGS cells. In male germ cells, genomic imprinting is erased during the fetal stage, and male-specific imprinting begins to be acquired around birth in prospermatogonia and is completed after birth (Davis et al., 1999, 2000; Kafri et al., 1992). While GS cells had a typical androgenetic imprinting pattern, the imprinting pattern of mGS cells clearly differed from those of androgenetic germ cells or somatic cells, which suggested that mGS cells originate from partially androgenetic germ cells that have undergone imprint erasure.

Another possibility is that mGS cells are derived from spermatogonial stem cells and that the ability to become multipotential cells may be one of the general character-

Table 2. Contribution of ES-Like Cells to Embryonic Development

Type of Cells	Number of Embryos Transferred	Number of Recipients	Number of Pups Born[a]	Number of Live Pups[b]	Chimera (%)	
					Male	Female
ES-like	193	11	54	36	9/22 (41)	4/14 (29)
ES	91	14	14	4	2/2 (100)	2/2 (100)
GS	124	7	28	16	0/8 (0)	0/8 (0)
4n rescue ES-like	92	4	0	NA	NA	NA
4n rescue ES	30	2	0	NA	NA	NA

NA, not applicable.
[a] In some experiments, fetuses were delivered by cesarean section at 19.5 dpc.
[b] Number of live pups on the next day after birth.

istics of germline cells. Possibly, the interaction with Sertoli cells normally directs germ cells to spermatogenesis and inhibits multilineage differentiation in the testis. However, when germline cells are continuously stimulated to expand in the absence of Sertoli cells, as in our culture conditions, germ cells may be released from this inhibition and some of the cells converted to pluripotent cells. Teratogenesis from germline cells is susceptible to environmental influences; for example, teratoma formation can be significantly enhanced (~10-fold) in vivo by ectopic transplantation of the fetal genital ridge (Stevens, 1984). As PGCs can become pluripotential only after in vitro culture and cytokine supplementation was also necessary for EG cell conversion (Matsui et al., 1992; Resnick et al., 1992), growth stimulation and release from somatic cells may modify the differentiation program of germline cells.

Several lines of evidence in our study provide support for the multipotential nature of spermatogonial stem cells. First, we did not find PGC-like germ cells in the neonatal testis, and we failed to induce mGS cells from neonatal testis in EG cell culture conditions (mSCF + LIF + bFGF). Therefore, the mGS cells arose through a different mechanism from that of EG cells, and the results suggest that PGC-like cells in neonatal testis, if any, are not responsible for the generation of mGS cells. Second, results of p53 knockout mouse experiments showed that mGS cells develop from GS cells. The use of the p53 knockout mouse was based on previous studies that showed an increased frequency of teratoma in this strain; it is estimated that loss of the *p53* gene results in a 100-fold increase in the susceptibility to testicular teratoma (Lam and Nadeau, 2003). Nevertheless, GS cells from this strain were phenotypically similar to wild-type spermatogonia and could produce normal-appearing spermatogenesis when transferred into seminiferous tubules. In this sense, they are indistinguishable from wild-type GS cells and fulfill the criteria for spermatogonial stem cells. Using this model, we found that the partial androgenetic imprint in mGS cells occurred with loss of the androgenetic imprint in GS cells. Perhaps the same is true of wild-type mGS cells; the partial androgenetic imprint patterns may not indicate the origin of mGS cells directly but rather reflect epigenetic instability in vitro, as reported for ES/EG cells (Labosky et al., 1994; Dean et al., 1998; Humpherys et al., 2001). Although these results are based on a mutant mouse model, they strongly suggest that GS cells are multipotential or can acquire multipotentiality by loss of a single gene. Spontaneous teratomas in mice occur almost exclusively in the 129/Sv background and are considered to develop from PGCs (Stevens, 1984). However, our results strongly suggest that spermatogonial stem cells are multipotential.

Interestingly, the acquisition of multipotentiality in mGS cells was concurrent with the loss of spermatogonial stem cell potential. Despite their testicular origin, mGS cells formed teratomas in the seminiferous tubules, indicating that this environment was no longer sufficient for spermatogenesis after the cells became pluripotent. This contrasts with GS cells, which produce spermatogenesis on transfer to the seminiferous tubules (Kanatsu-Shinohara et al., 2003a). Therefore, mGS cells are more closely related to ES/EG cells in terms of cell function. The reason for the loss of spermatogonial stem cell potential is unknown; however, we speculate that it may be related to the loss of responsiveness to GDNF during the course of the establishment of mGS cells, as GDNF is essential for the self-renewing division of spermatogonial stem cells (Meng et al., 2000). Another question that remains to be answered is why GS cells converted to mGS cells only at early passages. In our experiments, mGS cells appeared within 7 weeks of culture initiation but not at later stages. Once established, however, GS cells were stably committed to the germline, because we did not observe any mGS cell conversion when they were expanded in large-scale culture or transplanted in vivo. The loss of multipotentiality might be ascribed to the nonoptimal culture condition; it is widely known that ES cells differentiate easily and lose germline potential in the absence of LIF (Smith, 2001). Likewise, germline cells may tend to lose somatic cell potential in nonoptimal culture conditions. In this sense, it is interesting that, in contrast to mGS cells from wild-type mice, mGS cells developed in the long-term in p53 knockout mice. Although the mechanism for the maintenance or loss of multipotentiality of germline cells is currently unclear, the results suggest that this gene is involved in these processes, and GS cells from p53 knockout mice may be useful for analyzing how germline cells retain multipotentiality.

The most striking result from our experiments is the contribution of mGS cells to normal embryo development. Donor cell makers were present in various parts of the body, including the germline cells. These results demonstrate that mGS cells not only produce tumors but also can contribute to normal embryonic development. However, the function of the cells may not be completely

normal, because we could not recover live offspring in tetraploid complementation experiments, which indicates that mGS cells alone cannot produce a normal whole embryo. The failure is most likely related to the imprint status of mGS cells, since altered imprinted gene methylation causes fetal abnormalities with ES cells (Dean et al., 1998; Surani, 2001). Nevertheless, the imprint status of mGS cells did not influence the germline competence, and normal offspring were obtained from the chimeric animal. This agrees with the previous reports that both ES and EG cells can produce germline chimera (Robertson and Bradley, 1986; Labosky et al., 1994; Stewart et al., 1994), even with androgenetic imprint patterns (Narasimha et al., 1997).

The derivation of multipotent stem cells from the neonatal testis may have practical value for medicine and biotechnology. These cells are different from other reported multipotent cells in terms of morphology, marker expression, and capacity for differentiation (Verfaillie, 2002; Wagers and Weissman, 2004). While it is important to study the biology of individual cell types and assess their potential for clinical application, a major advantage of mGS cells is that techniques currently used to derive specific lineages of cells from ES cells are applicable directly. Clearly, the derivation of mGS cells has fewer ethical concerns than does the derivation of ES cells, because mGS cells can be obtained without sacrificing the conceptus or embryos. Furthermore, the availability of histocompatible, multipotent tissue for autotransplantation would circumvent immunological problems associated with ES cell-based technology. Although we failed to obtain mGS cells from mature wild-type animals, this was likely due to the low success rate of GS cell establishment. The results of the p53 knockout mouse experiment suggest that mGS cells can arise from mature testis. Development of more efficient systems to derive GS cells from mature testis is necessary at this stage of research, and suppression of p53 expression in GS cells, such as by RNA interference, may be useful for enhancing the frequency of derivation. Future studies should also be directed toward examining the effect of imprinting on the range and efficiency of differentiation. Such studies will provide important information for potential clinical applications.

Experimental Procedures

Cell Culture

Testis cells were collected from newborn (0–2 days old) ddY or DBA/2 mice (Japan SLC, Shizuoka, Japan). For some experiments, testis cells were collected from a newborn Green mouse (Kanatsu-Shinohara et al., 2003a) or p53 knockout mouse in ICR background (Tsukada et al., 1993). Testis cell culture was performed according to the previously published protocol (Kanatsu-Shinohara et al., 2003a), with slight modifications. In brief, testis cells were allocated to a gelatin-coated tissue culture plate (2×10^5 cells/3.8 cm^2). The next day, floating cells were recovered and passed to secondary culture plates. After 7 days in culture, the cells were passed to a fresh culture plate at a 1:2 dilution. When the cells were confluent (~7 days after the second passage), they were passed again (1:1 dilution). At the third or fourth passage, the cells were maintained on mitomycin C-inactivated MEF. ES-like cells were cultured in Dulbecco's modified Eagle's medium supplemented with 15% FCS, 5×10^{-5} M 2-mercaptoethanol, and 10^3 units/ml ESGRO (Invitrogen, Carlsbad, CA). To induce EG cells from neonatal testis, the same medium was also supplemented with 20 ng/ml human bFGF (Invitrogen), and cells were cultured on SI^4-m220 (gift from Dr. T. Nakano, Osaka University).

For adult testis culture, 2×10^7 cells from 3- to 8-week-old wild-type and p53 knockout mice were used to recover spermatogonial stem cells with anti-CD9 antibody as described elsewhere (Kanatsu-Shinohara et al., 2004), and selected cells were plated on gelatin-coated plate (3×10^5 cells/9.5 cm^2). GS cell colonies were picked by micromanipulation and transferred to MEF for expansion.

Standard ES cell medium was used to culture D3 ES cells that ubiquitously express the EGFP gene under the CAG promoter (provided by Dr. M. Okabe, Osaka University; Niwa et al., 1991).

Antibodies and Staining

The following primary antibodies were used: rat anti-EpCAM (G8.8), mouse anti-SSEA-1 (MC-480), mouse anti-sarcomeric protein (MF20; Developmental Studies Hybridoma Bank, University of Iowa), rat anti-mouse Forssman antigen (M1/87), rat anti-human α6-integrin (GoH3), biotinylated hamster anti-rat β1-integrin (Ha2/5), biotinylated rat anti-mouse CD9 (KMC8), allophycocyanin (APC)-conjugated rat anti-mouse c-kit (2B8), rat anti-mouse CD31 (MEC 13.3), phycoerythrin (PE)-conjugated rat anti-mouse Ter119 (TER-119), biotinylated rat anti-mouse Mac1 (M1/70), biotinylated rat anti-mouse Gr1 (RB6-8C5), rat anti-mouse VE-cadherin (11D4.1), APC-conjugated rat anti-mouse CD45 (30-F11; BD Biosciences), rat anti-TDA (EE2; provided by Dr. Y. Nishimune, Osaka University), APC-conjugated rat anti-mouse Flk-1 (Avas 12α1; provided by Dr. S. Nishikawa, RIKEN), goat anti-mouse cardiac troponin-I (cTn-I) (Santa Cruz Biotechnology, Santa Cruz, CA), mouse anti-human myosin light chain 2v (MLC2v) (Alexis Biochemicals Inc, Montreal, Canada), rabbit anti-mouse atrial natriuretic peptide (ANP) (Protos Biotech Corporation, NY), mouse anti-human myelin basic protein (MBP) (Pm43), rabbit anti-glial fibrillary acidic protein (GFAP), rabbit anti-mouse tyrosine hydroxylase (TH), and mouse anti-human β-tubulin III (Tuj) (SDL.3D10) (Sigma, St. Louis, MO). APC-conjugated goat anti-rat-IgG (Cedarlane Laboratories, ON, Canada), APC-conjugated streptavidin (BD Biosciences), Alexa Fluor 488-conjugated goat anti-mouse IgG, Alexa Fluor 647-conjugated goat anti-rat IgM, Alexa Fluor 633-conjugated goat anti-mouse IgM (Molecular Probes, Eugene, OR), Cy3-conjugated donkey anti-mouse IgG, Cy3-conjugated donkey anti-rabbit IgG, ALP or peroxidase-conjugated donkey anti-mouse IgG, ALP-conjugated donkey anti-rabbit IgG (Jackson Immunoresearch, West Grove, PA), ALP-conjugated rabbit anti-goat IgG (Vector Laboratories, Burlingame, CA), or ALP-conjugated goat anti-rat IgG (Chemicon) were used as secondary antibodies. The cell staining and analysis was carried out with a FACSCalibur system (BD Biosciences) (Kanatsu-Shinohara et al., 2003a). ALP or DAB staining was carried out using a VECTOR alkaline phosphatase substrate kit or DAB substrate kit (Vector Laboratories), respectively, according to manufacturer's protocol.

Differentiation into Specific Lineages In Vitro

For differentiation into mesodermal lineages, ES-like cells were cultured on OP9 feeder layers, and cell differentiation was induced as described (Nishikawa et al., 1998; Schroeder et al., 2003, Hirashima et al., 1999). Vascular cells were identified by the uptake of DiI-acetylated low-density lipoprotein (Molecular Probes). Methylcellulose culture was performed as described previously (Nishikawa et al., 1998). All cytokines were provided by Kirin Brewery (Tokyo, Japan). Neural cell differentiation was induced as previously described (Ying et al., 2003).

Analysis of Marker Gene Expression

RT-PCR for Nanog, Rex-1, ERas, Esg-1, Cripto, and ZFP57 were carried out using specific primers, as described (Mitsui et al., 2003; Goolsby et al., 2003; Takahashi et al., 2003; Tanaka et al., 2002; Kimura et al., 2001; Ahn et al., 2004). PCR amplifications for Oct-4, UTF1, and HPRT were carried out by using specific primers (5′-AGCTGCTGAAGCAGAAGAGG-3′ and 5′-GGTTCTCATTGTTGTCG GCT-3′ for Oct-4, 5′-GATGTCCCGGTGACTACGTCT-3′ and 5′-TCG GGGAGGATTCGAAGGTAT-3′ for UTF1, and 5′-GCTGGTGAAAAG GACCTCT -3′ and 5′- CACAGGACTAGAACACCTGC-3′ for HPRT).

Analysis of Imprinted Genes

Bisulfite genomic sequencing of DMRs of imprinted genes was carried out as described (Lee et al., 2002). PCR amplifications of each DMR region from bisulfite-treated genomic DNAs was carried out by using specific primers (5′-GGAATATTTGTGTTTTTGGAGGG-3′ and 5′-AATTTGGGTTGGAGATGAAAATATTG-3′ for *H19*, 5′-GGTTTGGTATATATGGATGTATTGTAATATAGG-3′ and 5′-ATAAAACACCAAATCTATACCAAAATATACC-3′ for *Meg3 IG*, 5′-GTGTAGAATATGGGGTTGTTTTATATTG-3′ and 5′-ATAATACAACAACAACAATAACAATC-3′ for *Rasgrf1*, 5′-TTAGTGGGGTATTTTTATTTGTATGG-3′ and 5′-AAATATCCTAAAAATACAAACTACACAA-3′ for *Igf2r*, 5′-GTAAAGTGATTGGTTTTGTATTTTTAAGTG-3′ and 5′-TTAATTACTCTCCTACAACTTTCCAAATT-3′ for *Peg10*, and 5′- GGTTTTTTAGAG GATGGTTGAGTG-3′ and 5′- TCCAACCCTACTAACCCATCACC-3′ for *Oct-4*). The DNA sequences were determined in both directions. For COBRA, PCR products were digested with restriction enzymes with a recognition sequence containing CpG in the original unconverted DNA (Xiong and Laird, 1997). Intensity of digested DNA bands was quantified with ImageGauge software (Fuji Photo Film, Tokyo, Japan).

Transplantation

For subcutaneous injections, approximately 2×10^6 cells were injected into KSN nude mice (Japan SLC). For microinjections into the seminiferous tubules, approximately 3×10^5 cells were injected into the seminiferous tubules of an immune-suppressed W mouse (Japan SLC) recipient through the efferent duct (Kanatsu-Shinohara et al., 2003b).

Chimera Formation and Microinsemination

Cells were injected into the blastocoel of 3.5 dpc blastocysts of C57BL/6 mice using a Piezo-driven micromanipulator (Kimura and Yanagimachi, 1995). The blastocysts were returned to the oviducts or uteri of 2.5 dpc pseudopregnant ICR foster mothers on the day of microinjection. Tetraploid embryo aggregation chimeras were produced using the method developed by Nagy et al. (1993), except that two-cell blastomeres were electrofused by applying an electric pulse (2500 V/cm, 10 μsec) in 300 mM mannitol solution. Microinsemination was carried out as described using BDF1 oocytes (Kimura and Yanagimachi, 1995). The embryos were transferred on the next day after culture.

Histology

Tissues were fixed in 10% formalin and processed for paraffin sectioning. Chimeric embryos were fixed in 4% paraformaldehyde and frozen in Tissue-Tek OCT compound (Sakura Finetechnical, Tokyo, Japan) for cryosectioning. Slides were analyzed with an Olympus confocal laser scanning microscope.

Acknowledgments

We declare that none of the authors have a financial interest related to this work. We thank Drs. Y. Kaziro and Y. Matsui for discussion and encouragement, and Ms. A. Wada for technical assistance. Financial support for this research was provided by the Inamori Foundation; the Ministry of Health and Welfare; and the Ministry of Education, Culture, Sport, Science, and Technology of Japan.

Received: April 30, 2004
Revised: October 7, 2004
Accepted: November 2, 2004
Published: December 28, 2004

References

Ahn, J.-I., Lee, K.-H., Shin, D.-M., Shim, J.-W., Lee, J.-S., Chang, S.Y., Lee, Y.-S., Brownstein, M.J., Lee, S.-H., and Lee, Y.-S. (2004). Comprehensive transcriptome analysis of differentiation of embryonic stem cells into midbrain and hindbrain neurons. Dev. Biol. *265*, 491–501.

Anderson, R., Schaible, K., Heasman, J., and Wylie, C.C. (1999). Expression of the homophilic adhesion molecule, Ep-CAM, in the mammalian germ line. J. Reprod. Fertil. *116*, 379–384.

Brinster, R.L., and Avarbock, M.R. (1994). Germline transmission of donor haplotype following spermatogonial transplantation. Proc. Natl. Acad. Sci. USA *91*, 11303–11307.

Brinster, R.L., and Zimmermann, J.W. (1994). Spermatogenesis following male germ-cell transplantation. Proc. Natl. Acad. Sci. USA *91*, 11298–11302.

Chambers, I., Colby, D., Robertson, M., Nichols, J., Lee, S., Tweedie, S., and Smith, A. (2003). Functional expression cloning of Nanog, a pluripotency sustaining factor in embryonic stem cells. Cell *113*, 643–655.

Davis, T.L., Trasler, J.M., Moss, S.B., Yang, G.J., and Bartolomei, M.S. (1999). Acquisition of the H19 methylation imprint occurs differentially on the parental alleles during spermatogenesis. Genomics *58*, 18–28.

Davis, T.L., Yang, G.J., McCarrey, J.R., and Bartolomei, M.S. (2000). The H19 methylation imprint is erased and re-established differentially on the parental alleles during male germ cell development. Hum. Mol. Genet. *9*, 2885–2894.

Dean, W., Bowden, L., Aitchison, A., Klose, J., Moore, T., Menesses, J.J., Reik, W., and Feil, R. (1998). Altered imprinted gene methylation and expression in completely ES cell-derived mouse fetuses: association with aberrant phenotypes. Development *125*, 2273–2282.

de Rooij, D.G., and Russell, L.D. (2000). All you wanted to know about spermatogonia but were afraid to ask. J. Androl. *21*, 776–798.

Evans, M.J., and Kaufman, M.H. (1981). Establishment in culture of pluripotential cells from mouse embryos. Nature *292*, 154–156.

Goolsby, J., Marty, M.C., Heletz, D., Chiappelli, J., Tashko, G., Yarnell, D., Fishman, P.S., Dhib-Jalbut, S., Bever, C.T., Jr., and Trisler, D. (2003). Hematopoietic progenitors express neural genes. Proc. Natl. Acad. Sci. USA *100*, 14926–14931.

Hattori, N., Nishino, K., Ko, Y.-G., Hattori, N., Ohgane, J., Tanaka, S., and Shiota, K. (2004). Epigenetic control of mouse Oct-4 gene expression in embryonic stem cells and trophoblast stem cells. J. Biol. Chem. *279*, 17063–17069.

Hirashima, M., Kataoka, H., Nishikawa, S., Matsuyoshi, N., and Nishikawa, S.-I. (1999). Maturation of embryonic stem cells into endothelial cells in an in vitro model of vasculogenesis. Blood *93*, 1253–1263.

Humpherys, D., Eggan, K., Akutsu, H., Hochedlinger, K., Rideout, W.M., III, Biniszkiewicz, D., Yanagimachi, R., and Jaenisch, R. (2001). Epigenetic instability in ES cells and cloned mice. Science *293*, 95–97.

Kafri, T., Ariel, M., Brandeis, M., Shemer, R., Urven, L., McCarrey, J.R., Ceder, H., and Razin, A. (1992). Developmental pattern of gene-specific DNA methylation in the mouse embryo and germ line. Genes Dev. *6*, 705–714.

Kanatsu, M., and Nishikawa, S.-I. (1996). In vitro analysis of epiblast tissue potency for hematpoietic cell differentiation. Development *122*, 823–830.

Kanatsu-Shinohara, M., Ogonuki, N., Inoue, K., Miki, H., Ogura, A., Toyokuni, S., and Shinohara, T. (2003a). Long-term proliferation in culture and germline transmission of mouse male germline stem cells. Biol. Reprod. *69*, 612–616.

Kanatsu-Shinohara, M., Ogonuki, N., Inoue, K., Ogura, A., Toyokuni, S., Honjo, T., and Shinohara, T. (2003b). Allogeneic offspring produced by male germ line stem cell transplantation into infertile mouse testis. Biol. Reprod. *68*, 167–173.

Kanatsu-Shinohara, M., Toyokuni, S., and Shinohara, T. (2004). CD9 is a surface marker on mouse and rat male germline stem cells. Biol. Reprod. *70*, 70–75.

Kimura, Y., and Yanagimachi, R. (1995). Mouse oocytes injected with testicular spermatozoa or round spermatids can develop into normal offspring. Development *121*, 2397–2405.

Kimura, C., Shen, M.M., Takeda, N., Aizawa, S., and Matsuo, I. (2001). Complementary functions of Otx2 and Cripto in initial patterning of mouse epiblast. Dev. Biol. *235*, 12–32.

Koshimizu, U., Nishioka, H., Watanabe, D., Dohmae, K., and Nishimune, Y. (1995). Characterization of a novel spermatogenic cell antigen specific for early stages of germ cells in mouse testis. Mol. Reprod. Dev. *40*, 221–227.

Labosky, P.A., Barlow, D.P., and Hogan, B.L.M. (1994). Mouse embryonic germ (EG) cell lines: transmission through the germline and differences in the methylation imprint of insulin-like growth factor 2 receptor (Igf2r) gene compared with embryonic stem (ES) cell lines. Development *120*, 3197–3204.

Lam, M.-Y.J., and Nadeau, J.H. (2003). Genetic control of susceptibility to spontaneous testicular germ cell tumors in mice. APMIS *111*, 184–191.

Lee, J., Inoue, K., Ono, R., Ogonuki, N., Kohda, T., Kaneko-Ishino, T., Ogura, A., and Ishino, F. (2002). Erasing genomic imprinting memory in mouse clone embryos produced from day 11.5 primordial germ cells. Development *129*, 1807–1817.

Liu, X., Wu, H., Loring, J., Hormuzdi, S., Disteche, C.M., Bornstein, P., and Jaenisch, R. (1997). Trisomy eight in ES cells is a common potential problem in gene targeting and interferes with germ line transmission. Dev. Dyn. *209*, 85–91.

Longo, L., Bygrave, A., Grosveld, F.G., and Pandolfi, P.P. (1997). The chromosome make-up of mouse embryonic stem cells is predictive of somatic and germ cell chimaerism. Transgenic Res. *6*, 321–328.

Martin, G.R. (1981). Isolation of a pluripotent cell line from early mouse embryos cultured in medium conditioned by teratocarcinoma stem cells. Proc. Natl. Acad. Sci. USA *78*, 7634–7638.

Matsui, Y., Zsebo, K., and Hogan, B.L.M. (1992). Derivation of pluripotential embryonic stem cells from murine primordial germ cells in culture. Cell *70*, 841–847.

Meistrich, M.L., and van Beek, M.E.A.B. (1993). Spermatogonial stem cells. In Cell and Molecular Biololgy of the Testis, C. Desjardins, and L.L. Ewing, eds. (New York: Oxford University Press), pp. 266–295.

Meng, X., Lindahl, M., Hyvönen, M.E., Parvinen, M., de Rooij, D.G., Hess, M.W., Raatikainen-Ahokas, A., Sainio, K., Rauvala, H., Lakso, M., et al. (2000). Regulation of cell fate decision of undifferentiated spermatogonia by GDNF. Science *287*, 1489–1493.

Mitsui, K., Tokuzawa, Y., Itoh, H., Segawa, K., Murakami, M., Takahashi, K., Maruyama, M., Maeda, M., and Yamanaka, S. (2003). The homeoprotein Nanog is required for maintenance of pluripotency in mouse epiblast and ES cells. Cell *113*, 631–642.

Nagy, A., Rossant, J., Nagy, R., Abramow-Newerly, A., and Roder, J.C. (1993). Derivation of completely cell culture-derived mice from early-passage embryonic stem cells. Proc. Natl. Acad. Sci. USA *90*, 8424–8428.

Nakano, T., Kodama, H., and Honjo, T. (1994). Generation of lymphohematopoietic cells from embryonic stem cells in culture. Science *265*, 1098–1101.

Narasimha, M., Barton, S.C., and Surani, M.A. (1997). The role of the paternal genome in the development of the mouse germ line. Curr. Biol. *7*, 881–884.

Nishikawa, S.-I., Nishikawa, S., Hirashima, M., Matsuyoshi, N., and Kodama, H. (1998). Progressive lineage analysis by cell sorting and culture identifies FLK1^{+}VE-cadherin^{+} cells at a diverging point of endothelial and hemopoietic lineages. Development *125*, 1747–1757.

Niwa, H., Yamamura, K., and Miyazaki, J. (1991). Efficient selection for high-expression transfectants with a novel eukaryotic vector. Gene *108*, 193–200.

Okuda, A., Fukushima, A., Nishimoto, M., Orimo, A., Yamagishi, T., Nabeshima, Y., Kuro-o, M., Nabeshima, Y., Boon, K., Keaveney, M., et al. (1998). UTF1, a novel transcriptional coactivator expressed in pluripotent embryonic stem cells and extra-embryonic cells. EMBO J. *17*, 2019–2032.

Pesce, M., and Schöler, H.R. (2001). Oct-4: gatekeeper in the beginning of mammalian development. Stem Cells *19*, 271–278.

Resnick, J.L., Bixler, L.S., Cheng, L., and Donovan, P.J. (1992). Long-term proliferation of mouse primordial germ cells in culture. Nature *359*, 550–551.

Robertson, E.J., and Bradley, A. (1986). Production of permanent cell lines from early embryos and their use in studying developmental problems. In Experimental Approaches to Mammalian Embryonic Development, J. Rossant, and R.A. Pedersen, eds. (Cambridge: Cambridge University Press), pp. 475–508.

Schrans-Stassen, B.H.G.J., van de Kant, H.J.G., de Rooij, D.G., and van Pelt, A.M.H. (1999). Differential expression of c-kit in mouse undifferentiated and differentiating type A spermatogonia. Endocrinology *140*, 5894–5900.

Schroeder, T., Fraser, S.T., Ogawa, M., Nishikawa, S., Oka, C., Bornkamm, G.W., Nishikawa, S.-I., Honjo, T., and Just, U. (2003). Recombination signal sequence-binding protein Jκ alters mesodermal cell fate decisions by suppressing cardiomyogenesis. Proc. Natl. Acad. Sci. USA *100*, 4018–4023.

Smith, A.G. (2001). Embryo-derived stem cells: of mice and men. Annu. Rev. Cell Dev. Biol. *17*, 435–462.

Solter, D., and Knowles, B.B. (1978). Monoclonal antibody defining a stage-specific mouse embryonic antigen (SSEA-1). Proc. Natl. Acad. Sci. USA *75*, 5565–5569.

Stevens, L.C. (1984). Spontaneous and experimentally induced testicular teratomas in mice. Cell Differ. *15*, 69–74.

Stevens, L.C., and Mackensen, J.A. (1961). Genetic and environmental influences on teratocarcinoma in mice. J. Natl. Cancer Inst. *27*, 443–453.

Stewart, C.L., Gadi, I., and Bhatt, H. (1994). Stem cells from primordial germ cells can reenter the germline. Dev. Biol. *161*, 626–628.

Surani, M.A. (2001). Reprogramming of genome function through epigenetic inheritance. Nature *414*, 122–128.

Takahashi, K., Mitsui, K., and Yamanaka, S. (2003). Role of ERas in promoting tumor-like properties in mouse embryonic stem cells. Nature *423*, 541–545.

Tanaka, T.S., Kunath, T., Kimber, W.L., Jaradat, S.A., Stagg, C.A., Usuda, M., Yokota, T., Niwa, H., Rossant, J., and Ko, M.S.H. (2002). Gene expression profiling of embryo-derived stem cells reveals candidate genes associated with pluripotency and lineage specificity. Genome Res. *12*, 1921–1928.

Tsukada, T., Tomooka, Y., Takai, S., Ueda, Y., Nishikawa, S.-I., Yagi, T., Tokunaga, T., Takeda, N., Suda, Y., Abe, S., et al. (1993). Enhanced proliferative potential in culture of cells from p53-deficient mice. Oncogene *8*, 3313–3322.

Verfaillie, C.M. (2002). Adult stem cells: assessing the case for pluripotency. Trends Cell Biol. *12*, 502–508.

Wagers, A.J., and Weissman, I.L. (2004). Plasticity of adult stem cells. Cell *116*, 639–648.

Xiong, Z., and Laird, P.W. (1997). COBRA: a sensitive and quantitative DNA methylation assay. Nucleic Acids Res. *25*, 2532–2534.

Ying, Q.L., Stavridis, M., Griffiths, D., Li, M., and Smith, A. (2003). Conversion of embryonic stem cells into neuroectodermal precursors in adherent monoculture. Nat. Biotechol. *21*, 183–186.